THE ASTROPHYSICAL JOURNAL, 550:897–918, 2001 April 1

AN EXPLORATION OF THE PARADIGM FOR THE 2–3 HOUR PERIOD GAP IN CATACLYSMIC VARIABLES

STEVE B. HOWELL
Astrophysics Group, Planetary Science Institute, 620 North 6th Avenue, Tucson, AZ 85705

LORNE A. NELSON[1]
Canadian Institute for Theoretical Astrophysics University of Toronto, 60 St. George Street, Toronto, ON, Canada M5S 3H8

AND

SAUL RAPPAPORT
Department of Physics and Center for Space Research, Massachusetts Institute of Technology, Cambridge, MA 02139
Received 2000 April 20; accepted 2000 November 8

ABSTRACT

We critically examine the basic paradigm for the origin of the 2–3 hr period gap in cataclysmic variables (CVs), i.e., binary systems in which a white dwarf accretes from a relatively unevolved, low-mass donor star. The observed orbital period distribution for ~ 300 CVs shows that these systems typically have orbital periods, $P_{\rm orb}$, in the range of ~ 80 minutes to ~ 8 hr but a distinct dearth of systems with $2 \lesssim P_{\rm orb}({\rm hr}) \lesssim 3$. This latter feature of the period distribution is often referred to as the "period gap." The conventional explanation for the period gap involves a thermal bloating of the donor star for $P_{\rm orb} \gtrsim 3$ hr due to mass transfer rates that are enhanced over those that could be driven by gravitational radiation (GR) losses alone (e.g., magnetic braking). If for some reason the supplemental angular momentum losses become substantially reduced when $P_{\rm orb}$ decreases below ~ 3 hr, the donor star will relax thermally and shrink inside of its Roche lobe. This leads to a cessation of mass transfer until GR losses can bring the system into Roche lobe contact again at $P_{\rm orb} \sim 2$ hr. We carry out an extensive population synthesis study of CVs, starting from $\sim 3 \times 10^6$ primordial binaries and evolving some $\sim 2 \times 10^4$ surviving systems through their CV phase. In particular we study current-epoch distributions of CVs in the $\dot{M}$-$P_{\rm orb}$, R_2-$P_{\rm orb}$, M_2-$P_{\rm orb}$, q-$P_{\rm orb}$, $T_{\rm eff}$-$P_{\rm orb}$, and L_2-$P_{\rm orb}$ planes, where $\dot{M}$ is the mass transfer rate, q is the mass ratio M_2/M_1, and M_2, R_2, $T_{\rm eff}$, and L_2 are the donor star mass, radius, effective temperature, and luminosity, respectively. This work presents a new perspective on theoretical studies of the long-term evolution of CVs. In particular, we show that if the current paradigm is correct, the secondary masses in CVs just above the period gap should be as much as $\sim 50\%$ lower than would be inferred if one assumes a main-sequence radius-mass relation for the donor star. We quantify the M_2-$P_{\rm orb}$ relations expected from models wherein the donor stars are thermally bloated. Finally, we propose specific observations, involving the determination of secondary masses in CVs, that would allow for a definitive test of the currently accepted model (i.e., interrupted thermal bloating) for the period gap in CVs.

Subject headings: binaries: close — novae, cataclysmic variables — stars: evolution — stars: low-mass, brown dwarfs — stars: mass loss

1. INTRODUCTION

Cataclysmic variables (CVs) are short-period binary systems consisting of a white dwarf that accretes matter via Roche lobe overflow from a low-mass companion star. These objects exhibit a wide range of phenomenology, including optical flickering in nova-like systems, dwarf nova eruptions that are thought to be caused by thermal instabilities in the accretion disks, and classical nova explosions, which are thermonuclear runaways of the accreted matter on the white dwarf (see, e.g., Warner 1995). The range of observed phenomena depends on the mass transfer rate, the mass ratio of the stellar components, and the magnetic field strength of the accreting white dwarf. The orbital periods of the majority of CVs range from 8 hr down to about 78 minutes, but both longer and shorter period systems are known. In the former case, the donor stars are typically somewhat evolved, while in the latter case, the donor stars are hydrogen-exhausted. In this paper we focus on the gap that exists in the orbital period distribution of CVs in the range of $\sim$2–3 hr (see, e.g., Warner 1976; Rappaport, Verbunt, & Joss 1983, hereafter RVJ; Spruit & Ritter 1983; Hameury et al. 1988a; Warner 1995).

The overall evolution of CV binaries is thought to be fairly well understood. The widely accepted explanation for the period gap rests on a mechanism for extracting angular momentum from the binary orbit (e.g., via magnetic braking of the secondary) for periods down to ~ 3 hr, followed by a relatively substantial decrease in the angular momentum loss rate.[2] The donor star, which had been thermally "bloated" in response to the mass loss driven by the systemic angular momentum losses, is then able to relax inside of its Roche lobe, and mass transfer ceases. The donor star is then thought to reestablish Roche lobe contact by the time the orbital period has decreased to about 2 hr, after which mass transfer resumes. In this paper we critically examine this paradigm for the creation of the period gap. While most workers believe in the existence of the so-called 2–3 hr period gap, a few (e.g., Wickramasinghe & Wu 1994;

[1] Present address: Physics Department, Bishop's University, Lennoxville, QC J1M 1Z7, Canada.

[2] We note that this scenario does not require the angular momentum loss rate to drop suddenly. Instead, it requires only that the timescale over which the angular momentum loss rate decreases must be shorter than the thermal timescale of the donor.

Verbunt 1997 [but see also Warner 1995; Wheatley 1995]) have questioned its reality, especially when all types of CVs are considered; however, we adopt the view that the period gap is a real feature of the CV population as a whole and, as such, requires a theoretical explanation (with observational tests) within the context of their binary evolution. Finally in this regard we note a suggestion by Clemens et al. (1998) that the period gap results from a "kink" in the radius-mass relation for main-sequence stars at a mass of about ~ 0.25 $M_\odot$ (but see the rebuttal by Kolb, King, & Ritter 1998).

In § 2 we describe the conventional picture of the evolution of a typical CV, including the period gap, and show some illustrative examples of binary evolution calculations for individual systems. In § 3 we explore how the binary evolution alters the relations among mass, radius, and orbital period of the secondary star. Specifically we discuss how the main-sequence radius-mass relationship must be modified to include the addition of a "bloating factor" that accounts for the changes caused by departures from thermal equilibrium of the mass-losing secondary star. We derive semianalytic mass-period and radius-period relationships for CV secondaries. In § 4 we describe our population synthesis and binary evolution codes, while in § 5 we present results from our population synthesis study of CVs in which the binary parameters of the CVs at all phases of their evolution are explored. In § 6 we show how assumptions that the donor star has a main-sequence radius-mass relation can lead to large errors in the assignment of the constituent stellar masses, most notably within the orbital period range of 3–5 hr. This period range should encompass the maximum bloating exhibited by a CV secondary compared to a main-sequence star of the same mass. Also in § 6 we discuss some specific observational implications resulting from our theoretical work. In particular, we present a specific test for CVs just above the period gap, which will enable us, in principle, to distinguish unambiguously among different possible explanations for the period gap. Finally, we present our summary and conclusions in § 7.

2. STANDARD EVOLUTIONARY SCENARIO FOR CVs

In the conventional picture of CV evolution (see, e.g., Faulkner 1971; Paczyński & Sienkiewicz 1981; Rappaport, Joss, & Webbink 1982, hereafter RJW; RVJ; Spruit & Ritter 1983; Hameury et al. 1988a; Kolb 1993), the early phases are expected to be dominated by angular momentum losses due to magnetic braking via a magnetically constrained stellar wind from the donor star (see, e.g., Verbunt & Zwaan 1981; RVJ). In these early phases, mass transfer rates are typically $\sim 10^{-9}$ to 10^{-8} $M_\odot$ yr^{-1}, and orbital periods range from ~ 8 hr to ~ 3 hr, just at the upper edge of the period gap. At some point in the evolution, the secondary becomes completely convective (at ~ 0.23 $M_\odot$) and, in the currently accepted view, magnetic braking is assumed to be greatly reduced. The near cessation of magnetic braking reduces the mass transfer rate and allows the secondary to shrink toward its thermal equilibrium radius. This causes a period of detachment, during which $\dot{M}$ drops to essentially zero, which lasts until the Roche lobe shrinks sufficiently to bring the secondary back into contact with it, at an orbital period of ~ 2 hr. This is the commonly accepted explanation for the observed period gap between 2–3 hr in CVs (RVJ; Spruit & Ritter 1983).

When mass transfer recommences at $P_{\rm orb} \sim 2$ hr, it is then driven largely by gravitational radiation losses at rates of $\sim 10^{-10}$ $M_\odot$ yr^{-1}. As the orbit shrinks and the mass of the donor star decreases, the mass-loss timescale increases, but the thermal timescale, $\tau_{\rm KH}$, increases much faster, owing to its approximate $\sim M^{-2}$ dependence. Therefore, at some point the thermal timescale grows larger than the mass transfer timescale. When this occurs, the donor star is unable to adjust to the mass loss on its thermal timescale, and it therefore starts to expand upon further mass loss, in accordance with its adiabatic response; i.e., $[d\ln(R)/d\ln(M)]_{\rm ad} < 0$. Typically, at this point the orbital period is ~ 80 minutes and the mass of the donor star is ~ 0.06 $M_\odot$. From this point on, the mass of the donor star will continue to decrease (but with longer and longer $\dot{M}$ timescales), the orbital period will increase back toward periods approaching ~ 2 hr (within a Hubble time), and the interior of the donor star will become increasingly electron degenerate. A discussion of this later stage of CV evolution is presented by Howell, Rappaport, & Politano (1997, hereafter HRP).

To make these evolutionary descriptions somewhat more quantitative, we show in Figure 1 the secular evolution of several model CVs under the influence of magnetic braking and gravitational radiation. The evolution code used to generate these results is a descendant of the one used by RVJ and is described in § 4.2 along with recent improvements to the code. The two panels on the left-hand side of Figure 1 show the evolution with time of a CV binary with initial constituent masses of $M_2 = 0.9$ $M_\odot$ and $M_{\rm WD} = 1.1$ $M_\odot$, where M_2 and $M_{\rm WD}$ are the masses of the donor star and white dwarf, respectively. Other parameters used in the calculation are for our "standard model" (see Table 1 for definitions). The top and bottom panels show the evolution with time of the mass transfer rate and orbital period, respectively, for an assumed donor star with solar composition. The calculations have been carried out to approximately the age of the Galaxy. The evolutionary phases and features discussed above are present in Figure 1, including the interval where mass transfer is driven by magnetic braking ($\sim 10^{7.3}$–$10^{8.4}$ yr), the period gap ($\sim 10^{8.4}$–$10^{8.8}$ yr), the interval where $\dot{M}$ is driven by gravitational radiation losses ($> 10^{8.8}$ yr), the period minimum at $10^{9.4}$ yr, the subsequent increase in $P_{\rm orb}$ back up to ~ 2 hr, and the sharp falloff in $\dot{M}$ after orbital period minimum.

On the right-hand side of Figure 1 the temporal evolution of four other illustrative model CV binaries are shown. The following discussion contains descriptions of the period gap that develops in these systems; these are easier to visualize by looking also at Figure 2. The initial masses

TABLE 1

SUMMARY OF MODEL PARAMETERS

Model	β[a]	α[b]	γ[c]	$C_{\rm MB}$[d]
A. Standard model	0	1	3	1
B. Reduced magnetic braking	0	1	3	1/2
C. High angular momentum losses	0	2	3	1
D. Conservative mass transfer	1	...	3	1

[a] Fraction of mass lost by the donor star that is transferred to, and ultimately retained by, the white dwarf.

[b] Specific angular momentum carried away in nova explosions in units of the specific angular momentum of the white dwarf.

[c] Magnetic braking parameter γ as defined in RVJ.

[d] Proportionality constant in the magnetic braking expression used by RVJ, in units of their "standard" value.

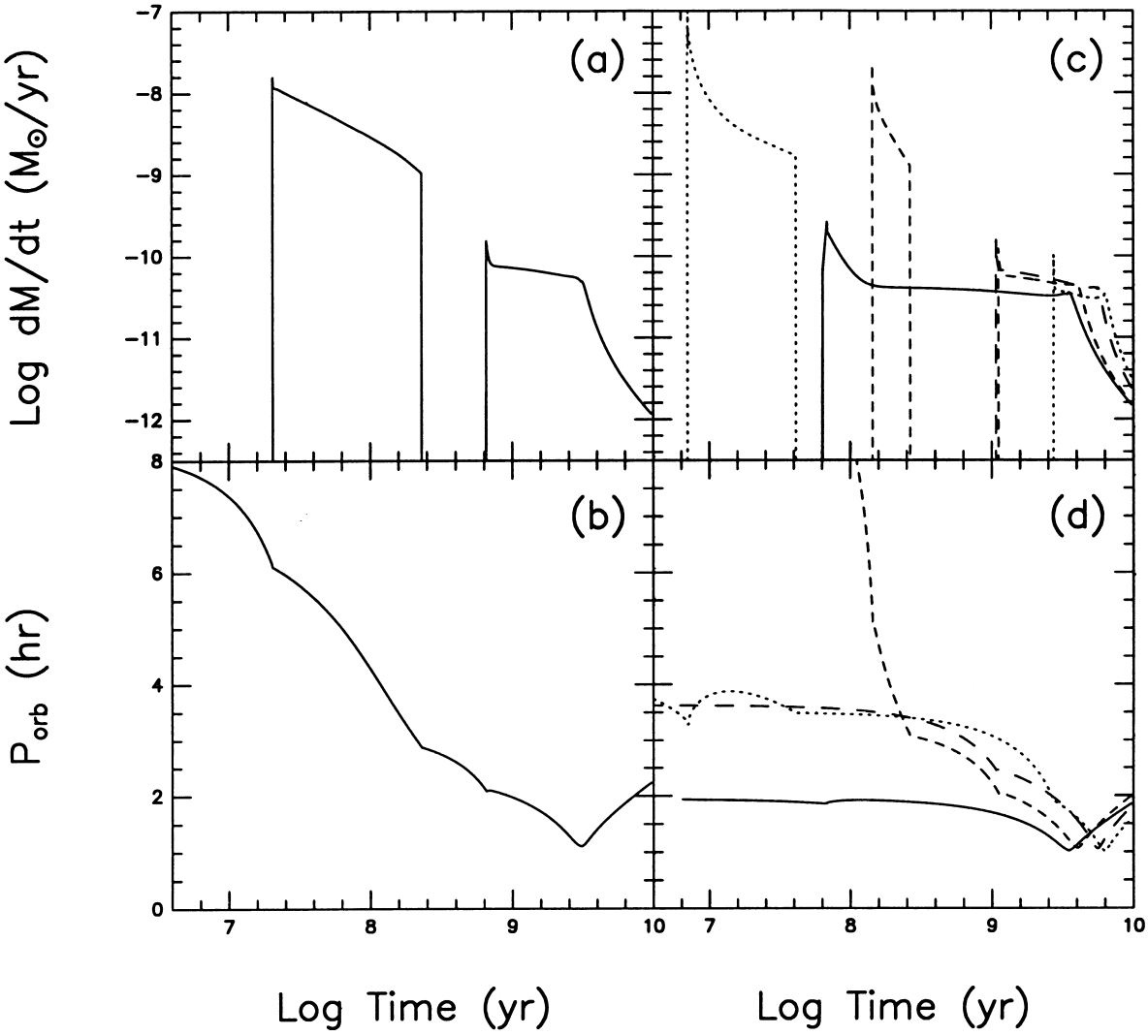

FIG. 1.—Evolution with time of the mass transfer rate, $\dot{M}$, and orbital period, $P_{\rm orb}$, for several model cataclysmic variable systems. *Left:* the evolution of a single CV with initial masses ($M_2 = 0.9\ M_\odot$; $M_{\rm WD} = 1.1\ M_\odot$). This system first comes into Roche lobe contact at $P_{\rm orb} = 6$ hr and evolves through the period gap to the minimum in $P_{\rm orb}$ and back up to longer periods by 10^{10} yr. *Right:* the evolutions of a selection of four other illustrative initial binary constituent masses, M_2, $M_{\rm WD} = 0.2, 0.4$ (*solid line*), 0.35, 0.35 (*dotted line*), 0.3, 0.6 (*dashed line*), and 0.65, 0.7 (*long-dashed lined*), all in units of $M_\odot$.

(M_2, $M_{\rm WD}$) of these systems are (0.2, 0.4), (0.35, 0.35), (0.3, 0.6), and (0.65, 0.7), all in units of $M_\odot$. For the system with initial masses (0.2, 0.4) the binary comes into Roche lobe contact for the first time at an orbital period below the gap, i.e., at $P_{\rm orb} = 2$ hr (Figs. 1*c* and 1*d*, *solid curves*). Note the enhanced mass transfer rate at ~ 30 Myr after Roche lobe contact is made. The subsequent evolution is not dissimilar to the one shown in the left-hand panels. For the system with initial masses (0.35, 0.35), the donor star commences mass transfer at a period of 3.3 hr, with magnetic braking still operative (Figs. 1*c* and 1*d*, *dotted curves*). Because the two masses are the same when the donor star first fills its Roche lobe, the mass transfer is only marginally stable (see the discussion in § 4.2 below). Therefore, $\dot{M}$ is initially very high and the system is quickly driven out of thermal equilibrium, causing the orbit to expand. This system comes out of contact (i.e., enters the period gap) at an orbital period of 3.5 hr. The system with initial masses (0.3, 0.6) is an example of one that commences mass transfer *in* the period gap. Lastly, the system with initial masses (0.65, 0.7) is another example of a system that exhibits the "usual" 2–3 hr period gap, but commences mass transfer at $P_{\rm orb} = 5$ hr.

In Figure 2 the same evolutions shown in Figure 1 are again presented, but this time the binary parameters are displayed as a function of the evolving orbital period. As in Figure 1, the left-hand panels are for initial masses (M_2, $M_{\rm WD}$) of (0.9, 1.1), while the right-hand panels are for initial masses of (0.2, 0.4), (0.35, 0.35), (0.3, 0.6), and (0.65, 0.7). The top, middle, and bottom panels show the evolution of $\dot{M}$, M_2, and R_2, respectively. As mentioned above, the period gap is more evident in Figure 2 than it is in Figure 1. We note here several unique features associated with the evolution of individual CVs; an understanding of these features will aid our interpretation of the results obtained for an entire population of evolving CV systems (see § 5). For example, $\dot{M}$ typically exhibits a sharp spike at the onset of mass transfer, (see also RVJ and Hameury et al. 1988b); this behavior will appear in all of the two-dimensional "images" we produce from the population synthesis calculations in § 5. The mass of the donor stays constant during its evolution through the period gap since there is no mass transfer taking place at that time—this is indicated by the horizontal lines in the middle panels. The abrupt shift in location between the M_2-$P_{\rm orb}$ track above the period gap

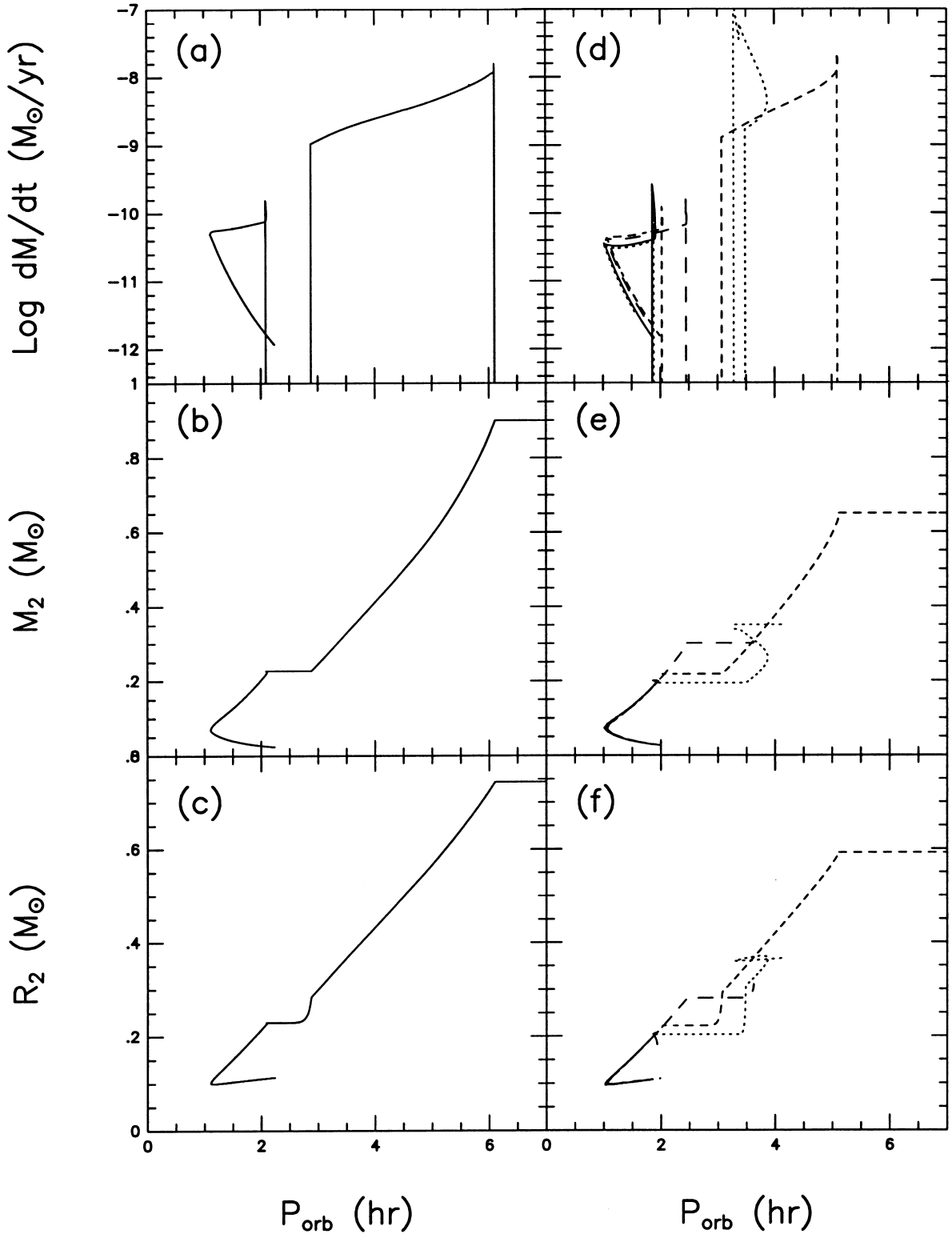

FIG. 2.—Evolution with orbital period, P_{orb}, of the mass transfer rate, $\dot{M}$, secondary mass, M_2, and secondary radius, R_2, for several illustrative model cataclysmic variable systems. The initial masses for the systems whose evolutions are displayed in the left and right sets of panels are the same as described in Fig. 1.

and below the gap will be dramatically apparent in the population synthesis results and will have important consequences that are discussed below. Finally, the radius of the donor star decreases sharply after the system enters the period gap; in fact, it is the shrinking of the donor inside of its Roche lobe when the magnetic braking ceases that is the putative cause of the period gap. Again, the abrupt shift between the R_2-P_{orb} track above and below the period gap will be very pronounced in the population synthesis results.

A noteworthy feature of Figures 1*a*, 1*c*, 2*a*, and 2*d* mentioned above is the sharp rise in $\dot{M}$ whenever mass transfer has just commenced, including the first time that the donor star fills its Roche lobe and after the resumption of mass transfer below the period gap. This results from the fact that

when a low-mass star (i.e., $\lesssim 0.5\ M_\odot$) is in thermal equilibrium (i.e., the nuclear luminosity, $L_{\rm nuc}$, equals the bolometric luminosity, $L_{\rm opt}$), the sudden onset of mass transfer forces the star to expand because its adiabatic index is negative (discussed above). This expansion can cause a temporarily anomalously high rate of mass transfer, viz., the episodes of high $\dot{M}$ seen in Figures 1*a*, 1*c*, 2*a*, and 2*d*. However, as soon as the donor star expands, its core temperature drops slightly, and $L_{\rm nuc}$, which is a highly sensitive function of temperature, drops dramatically. This leads to a luminosity deficit wherein $L_{\rm nuc} < L_{\rm opt}$. The star can then lose a net amount of energy, shrink, and approach its new thermal equilibrium radius (appropriate to its lower mass) on a Kelvin-Helmholtz (i.e., thermal) timescale. During the mass-loss process, true thermal equilibrium is never reached, and the luminosity deficit attains a value that is adequate to allow the star to shrink continuously. The above discussion explains the transient episodes of higher transfer rates at the start of mass transfer epochs and the "outlying" lower probability CV states we shall encounter in § 5. It also explains the thermal "bloating" of the donor star, which is discussed in § 3 and will play a key role in the observational test we propose in § 6. (For earlier discussions of some of these basic effects, see RJW and Hameury et al. 1988a.)

The five individual evolutions shown in Figures 1 and 2 serve to illustrate the range of interesting possibilities for CVs that commence mass transfer with different mass ratios. The population synthesis study described in § 5 explores these various possibilities in a more systematic and complete way.

3. QUANTITATIVE EFFECTS OF THERMAL BLOATING OF THE SECONDARY STAR

We start with the assumption that during mass transfer in a CV the Roche lobe of the donor star is located within its atmosphere, i.e., the donor star is "filling" its Roche lobe (see Howell et al. 2000). We then take the Roche lobe radius of the secondary star to be given by the simple expression of Kopal (1959):

$$R_2 \simeq 0.46a\left(\frac{M_2}{M_2 + M_{\rm WD}}\right)^{1/3} . \quad (1)$$

This can be combined with Kepler's third law to yield the well-known relationship among the mass, radius, and orbital period of the donor star:

$$P_{\rm orb}(M_2, R_2) \simeq 9M_2^{-1/2}R_2^{3/2} , \quad (2)$$

where M_2, R_2, and $P_{\rm orb}$ are expressed in units of $M_\odot$, $R_\odot$, and hours, respectively. If we now assume that the radius of the donor star is some factor f times the radius it would have if it were a normal main-sequence star, we can write

$$R_2 = faM_2^b , \quad (3)$$

where we approximate the radius-mass relation for stars on the lower main sequence (i.e., G to M stars) by $R_2 = aM_2^b$, where a and b are constants, and we refer to f as the "bloating factor." This bloating factor f is simply a measure of how much larger the radius of a CV secondary is than that of a single, main-sequence star of the same mass owing to the departure from thermal equilibrium. We can now combine equations (2) and (3) to derive relations for the mass and radius of CV secondaries as a function of the binary orbital period:

$$M_2 \simeq 9^{-2/(3b-1)}P_{\rm orb}^{2/(3b-1)}(af)^{-3/(3b-1)} , \quad (4)$$

$$R_2 \simeq 9^{-2b/(3b-1)}P_{\rm orb}^{2b/(3b-1)}(af)^{-1/(3b-1)} . \quad (5)$$

For the purposes of this exercise, we take $a = 0.85$ and $b = 0.85$, which we find by fitting a power law to the main-sequence models of Dorman, Nelson, & Chau (1989, hereafter DNC). With these values for the constants a and b, the above equations simplify to

$$M_2(P_{\rm orb}) \simeq 0.08f^{-1.95}P_{\rm orb}^{1.3} , \quad (6)$$

$$R_2(P_{\rm orb}) \simeq 0.10f^{-0.65}P_{\rm orb}^{1.1} , \quad (7)$$

where, again, M_2 and R_2 are in solar units and $P_{\rm orb}$ is in hours. The conclusions drawn from these expressions are somewhat counterintuitive in that, for a CV at a given orbital period, if the donor star is *bloated*, the proper radius and mass that should be inferred from the orbital period are *smaller* than the values that would be inferred if the star were on the main sequence (see also Beuermann et al. 1998). In § 6 we derive polynomial fits for $M_2(P_{\rm orb})$ and $R_2(P_{\rm orb})$ from our population synthesis study; the analytic expressions given by equations (6) and (7) serve mainly to demonstrate how these quantities scale with the bloating factor f.

4. POPULATION SYNTHESIS STUDY

The individual binary evolution runs shown in Figures 1 and 2 for several different combinations of initial constituent masses are instructive, but they do not (1) adequately sample the full range of possible initial masses or (2) provide us with the distributions of CV binary properties at the current epoch. We have therefore undertaken a population synthesis study of CVs that consists of two parts. In the first part, we utilize a Monte Carlo approach to select a large number ($\sim 3 \times 10^6$) of primordial binaries and follow the evolution of these systems to see which ones undergo a common envelope phase. In such events, the envelope of the giant star engulfs the secondary, leading to a spiral-in episode that leaves the secondary in a close orbit with a white dwarf (i.e., the core of the primary star; see, e.g., Paczyński 1976; Webbink 1979; see also § 4.1 for details). Primordial binaries that are too wide will not undergo any significant mass transfer and will not lead to the formation of CV systems—the evolution of such wide binaries is not followed in the present study. Successful systems that emerge from the first part of our population synthesis calculations are those that do undergo a common envelope phase and yield a close binary consisting of a white dwarf and low-mass ($\lesssim 1\ M_\odot$) companion. The second part of the population synthesis considers those white-dwarf main-sequence binaries for which systemic angular momentum losses, or a modest amount of evolution by the normal companion star, can initiate Roche lobe contact within a Hubble time. Each of these systems is then evolved in detail through the mass transfer phase (CV phase) until the donor star has been reduced to a negligible mass (typically 0.03 $M_\odot$).

A number of prior population synthesis studies of cataclysmic variables have been carried out. These include work by Politano (1988, 1996), de Kool (1992), Kolb (1993), Di Stefano & Rappaport (1994, for CVs in globular clusters), and HRP (emphasizing systems that evolve beyond the orbital period minimum). The current study has

several new features and advantages over the previous studies. First, we compute probability density functions in two parameters, e.g., $\dot{M}P_{\rm orb}$ and M_2:$P_{\rm orb}$ (see § 4.3). This way of studying and evaluating the results of population synthesis calculations has a distinct advantage over producing distributions of a single parameter. For example, we are able to quantitatively evaluate phases of the evolution that are short-lived or represent unusual evolutionary states (e.g., whenever Roche lobe contact has just been established or when the initial binary mass ratio is near unity). Other examples include the ability to discern the spread in $\dot{M}$ at a given orbital period, the distinction between systems with He and CO white dwarfs, and the pronounced depression in secondary mass at a given orbital period (for systems just above the period gap). A second advantage is that our code for evolving the donor stars was originally developed to evolve brown dwarfs of very low mass to very old ages. The code has been well "calibrated" against other more sophisticated ones that have been used for the purpose of evolving brown dwarfs (see § 4.1). Finally, our population synthesis code, which is used to generate the zero-age CVs that are input to the binary evolution code, provides an independent check on previous work and tests the sensitivity of our conclusions to various uncertainties in the physics, initial conditions, and other input parameters.

Finally, we mention a possibly important limitation on the study we present here, which also applies to most other prior work in this area. We have considered only donor stars with $M_2 \leq 1\ M_\odot$, and we do not allow for the chemical (nuclear) evolution the donor. The latter approximation is realistic if the donor star commences mass transfer within $\sim 3 \times 10^9$ yr of the common envelope event, or if the donor has a mass of $\lesssim 0.7\ M_\odot$. These conditions apply to most of the systems that successfully evolve through the CV phase in our calculations. Furthermore, we find that only $\sim 5\%$ of all the stable mass transferring, zero-age CVs in our population synthesis study have secondaries that are older than one-third of their main-sequence lifetime prior to the start of mass transfer. Theoretically, there should indeed be some CVs that evolve from donor stars that are initially more massive than $1\ M_\odot$, and they should be followed in future population synthesis studies. For the present study, we simply assume that such systems, with donors whose initial mass exceeds $1\ M_\odot$, do not contribute substantially to the CV population and, above all, would not affect our conclusions concerning systems near the period gap.

In this regard, recent work by Beuermann et al. (1998) examines the properties of the secondary star in CVs in an effort to determine whether they are indeed similar to normal main-sequence stars. They show that, in the spectral type–$P_{\rm orb}$ plane, the ~ 50 CVs with measured spectral types lie below the expected relation for main-sequence stars (i.e., they are cooler at a fixed value of $P_{\rm orb}$). Beuermann et al. conclude that for systems with $P_{\rm orb} < 6$ hr this effect could result from mass loss (see § 5) but that for longer orbital periods this effect suggests chemical evolution of the donor star. This is a potentially important finding for systems with orbital periods longer than we consider here and could also possibly impact the shorter period systems as well. From our population synthesis results, we find that $\sim 10\%$ of CVs could potentially form with progenitors whose mass is initially sufficiently high (i.e., $\gtrsim 1\ M_\odot$) that chemical evolution of the donor star might indeed be significant. Systems with such donor stars are not followed in the present study. If, for some as yet unknown reason, the more massive donor stars have a greater efficiency for producing CVs than their lower-mass counterparts, then chemical evolution may indeed prove influential in the evolution of CVs. These possibilities should be examined in future population synthesis studies.

4.1. *Choosing the Zero-Age CVs*

The properties of the primordial binary systems are chosen via Monte Carlo techniques as follows. The primary mass is picked from Eggleton's (2000) Monte Carlo representation of the Miller & Scalo (1979) initial mass function (IMF),

$$M_1(x) = 0.19x[(1 - x)^{3/4} + 0.032(1 - x)^{1/4}]^{-1}\ , \quad (8)$$

where x is a uniformly distributed random number. This distribution flattens out toward lower masses, in contrast with a Salpeter-type power-law IMF (1955). We considered primary stars whose mass is in the range of $0.8 < M_1 < 8\ M_\odot$. Next, the mass of the secondary, M_2, is chosen from the probability distribution, $f(q) = 5/4q^{1/4}$, where $q \equiv M_2/M_1$ (Abt & Levy 1978; but also see Halbwachs 1987). This mass ratio distribution is, at best, poorly known empirically. Our adopted distribution has the property that the mass of the secondary is correlated with the mass of the primary but is not strongly peaked toward $q = 1$. We find that our results are not very sensitive to the choice of $f(q)$, unless an extreme is adopted such as the assumption that the two masses are to be chosen completely independently of one another (see, e.g., Table 2 and Fig. 4 in Rappaport, Di Stefano, & Smith 1994, hereafter RDS). Secondary masses as small as $0.09\ M_\odot$ are chosen (we wanted to ensure that only stars with masses clearly above the minimum main-sequence mass are included). To choose an initial orbital period, a distribution that is uniform in log (P) over the period range of 1 day to 10^6 yr is used (see, e.g., Abt & Levy 1978; Duquennoy & Mayor 1991). Since we consider only circular orbits, the adopted orbital period distribution more properly pertains to the tidally circularized orbits than to the initial orbits of the primordial binaries.

After the masses and orbital period are chosen, the orbital separation is calculated using Kepler's third law. We utilize an analytic expression for the relation among the core mass, the radius, and the total mass of the primary to estimate the mass of the degenerate core, $M_{\rm WD}$, when the primary fills its Roche lobe. The expression we used for this purpose (see RDS) was designed to reproduce the features of Figure III.2 of Politano (1988) and Figure 1 of de Kool (1992), except that the core-mass radius relation for stars with mass $\lesssim 2\ M_\odot$ was renormalized to match the fitting formula of Eggleton (2000; see eq. [4] of Joss, Rappaport, & Lewis 1987). Mass loss via a stellar wind prior to the start of the first mass transfer phase was computed via an analytic expression derived by M. Politano (1999, private communication). In practice, the inclusion of this wind mass loss does not significantly affect the results.

In order to select only systems that undergo a common envelope phase we require that the radius of the Roche lobe of the primary be larger than the radius of a star of mass M_1 at the base of the giant branch (see, e.g., Paczyński 1965; Webbink 1979, 1985, 1992; de Kool 1992, and references therein). This ensures that unstable mass transfer will occur on a timescale that is substantially shorter than a thermal time and should lead to a common-envelope phase. Once

mass transfer from the primary to the secondary commences, we assume that a common envelope phase occurs and compute the final spiral-in separation based on simple energetic considerations (see, e.g., Taam, Bodenheimer, & Ostriker 1978; Meyer & Meyer-Hofmeister 1979; Livio & Soker 1988; Webbink 1992; RDS; Taam & Sandquist 1998). The expression we use for determining a_f, the final orbital separation after spiral-in, is given by

$$\frac{\epsilon G M_2}{2}\left(\frac{M_{\rm core}}{a_f}-\frac{M_1}{a_i}\right)=\frac{G M_{\rm env}(M_{\rm env}+3M_{\rm core})}{R_1}, \quad (9)$$

where $M_{\rm core}\equiv M_{\rm WD}$ and $M_{\rm env}$ are the core and envelope masses of the primary, R_1 is the radius of the primary, a_i is the initial orbital separation, and ϵ is the energy efficiency factor for ejecting the envelope. We take ϵ to have a value of 1.0 in our standard model. The two terms in parentheses on the right-hand side of equation (9) represent the binding energy of the envelope of the primary to itself and to its core. The dimensionless coefficients multiplying each term were computed for an assumed polytropic envelope structure with polytropic index $n = 3.5$ (RDS). For other similar values of n the ratio of $\sim 3{:}1$ between the two coefficients is roughly the same. We assume that the duration of the spiral-in is sufficiently short ($<10^4$ yr; see above references) that the mass of the secondary does not change significantly during the common envelope phase.

After the spiral-in episode, the separation, the white dwarf mass, the secondary mass, and the corresponding Roche lobe radius of the secondary are known. If at the end of the common envelope phase the secondary would already be overfilling its Roche lobe, then we eliminate the system. (In most cases, this circumstance would be expected to lead to a merger of the secondary star with the degenerate core of the primary, which presumably would result in the formation of a giant star.) In practice, if the Roche lobe is larger than $\sim 20\ R_\odot$, then neither magnetic braking nor gravitational radiation would bring the system into Roche lobe contact before the secondary would evolve past the base of the giant branch. We can also eliminate these systems since the ensuing mass transfer would either be dynamically unstable (see, e.g., Paczyński 1967; Kippenhahn, Kohl, & Weigert 1967; Webbink 1979, 1992) or lead to an even wider orbit; either case would not produce a CV of the ordinary kind.

We typically start with $(3\text{–}5) \times 10^6$ primordial binaries and end up with $\sim$15,000 pre-CVs to evolve through the mass transfer phase with the bipolytrope evolution code described in the next section. The computational time for this first portion of the calculations is negligibly short.

4.2. *Evolving the CVs through Their Mass Transfer Phase*

As mentioned earlier, the evolutionary tracks of CV systems are calculated using a version of the code that was first developed by RVJ (see also RJW) to explore the effects of the parameterized Verbunt & Zwaan (1981) magnetic braking law on the evolutionary properties of cataclysmic variables. According to their algorithm, the mass-losing donor is approximated by a bipolytrope wherein the convective envelope is represented by an $n = 3/2$ polytrope and the radiative core by an $n = 3$ polytrope. One of the advantages of this code is that it allows for the rapid computation of a large number of evolutionary tracks and provides a more physically intuitive interpretation of the results. The original version of the code has been modified substantially to allow for improvements to the input physics and to ensure that the conditions near the surface (atmosphere) are more physically realistic. A number of these changes have been discussed in previous papers.

The most significant of these modifications and updates are described by Nelson, Rappaport, & Joss (1986a, 1986b, 1993), who used a single polytrope model to follow the evolution of fully convective low-mass stars and brown dwarfs. The results of the brown dwarf cooling evolutions and the calculation of zero-age main-sequence (ZAMS) star models of low-mass stars are in excellent agreement with those calculated using more sophisticated techniques (see, e.g., DNC; Burrows et al. 1993, 1997; Baraffe et al. 1998, and references therein). Specifically, coulombic corrections to the pressure equation of state were incorporated and an updated version of the Alexander, Johnson, & Rypma (1983; D. R. Alexander 1989, private communication) low-temperature, radiative (surface) opacities was used. The molecular hydrogen partition function was also calculated more accurately. Most importantly, the specific entropy at the surface was matched directly to the specific entropy in the interior, i.e., at the interface between the radiative core and the convective envelope.[3]

In addition to these changes, the atmospheric pressure boundary condition was modified so as to approximate more closely the scaled solar T-τ (Krishna-Swamy 1972) relation. The radiative surface opacities did not include the effects of grain formation. Since grains can only form in the atmospheres of very low temperature stars ($\leq$1500 K), this should affect mostly the evolution of those CVs that have evolved beyond the orbital period minimum. However, we have found that the evolution of CVs through and beyond the period minimum is not particularly sensitive to this omission.

The overall result of all of these changes is that the theoretical radius-mass relation for our ZAMS models with masses $\leq 1.0\ M_\odot$ is now in substantial agreement with other theoretical calculations as well as with observational studies of low-mass stars (see DNC). For similar abundances of hydrogen and for stars of approximately solar metallicity, we find that the radii of our new models compared with other theoretical models (and the DNC results) typically agree to within an rms error of $\sim 3\%$ ($M \leq 1.0\ M_\odot$). Deviations among the theoretical models are greatest for the higher mass stars because of uncertainties in the mixing length parameter and the treatment of inefficient (superadiabatic) convection. When observations of double stars are considered, we believe that our ZAMS radii are accurate to within $\sim 5\%$. Our ZAMS models become fully convective at a mass of $\sim 0.34\ M_\odot$. This is considerably smaller than the value given in RVJ but agrees well with the DNC results (as well as with newer generations of models).

Mass transfer in CVs is driven by angular momentum losses due to gravitational radiation (Landau & Lifshitz 1962) and other systemic angular momentum losses such as "magnetic braking." The magnetic braking law that we

[3] A small entropy mismatch was introduced to correct for thin regions of superadiabatic convection/radiative transport that exist beneath the photosphere of the more massive stars in our mass range. These corrections depend on the assumed value of the mixing length parameter and were chosen so as to provide the best possible representations of ZAMS stars. They were largest for the 1.0 $M_\odot$ model ($\sim 5\%$ of the specific entropy), decreasing to zero for fully convective stars.

utilize is that of Verbunt & Zwaan (1981) and parameterized by RVJ. The magnetic braking parameters were chosen so as to best reproduce the observed period gap. According to the parameterization described in RVJ, we took $\gamma = 3$ and did *not* adjust the multiplicative constant (defined here as $C_{\rm MB}$) used in the RVJ prescription. We also "shut off" magnetic braking when the radiative core had been reduced to less than 15% of the mass of the donor. Magnetic braking is assumed to be greatly reduced as a result of the restructuring of the magnetic field of the donor star when it becomes nearly fully convective. This reduction in the angular momentum loss rate gives the donor an opportunity to shrink inside of its Roche lobe on a thermal timescale. Further angular momentum losses due to gravitational radiation cause mass transfer to recommence once the binary system is brought back into a state of semidetachment (see, e.g., RVJ; Spruit & Ritter 1983; Hameury et al. 1988a for a more detailed explanation). As pointed out in several places in this work, the actual mechanism that produces the bloating of the donor and the means by which mass transfer is interrupted are not central to the conclusions drawn in this paper. What is important in this regard is that the bloating be sufficiently large as to produce the observed width of the period gap. For our standard evolutionary model the period gap covers the range of $2.1 < P_{\rm orb} < 2.85$ hr. According to Warner (1995), this synthetic gap approximates the observed one very well.

We assume that mass and orbital angular momentum *are* lost as a result of nova explosions on the surface of the white dwarf accretor. For our standard model we assumed that all of the mass that is accreted by the white dwarf is lost with the same specific angular momentum as the white dwarf itself (see Schenker, Kolb, & Ritter 1992). Given the relatively low mass transfer rates, it is likely that the nova events are extremely hydrodynamic, and thus it is unlikely that any of the accreted mass actually contributes to increasing the mass of the white dwarf (see, e.g., Prialnik & Kovetz 1995; Starrfield 1998 and references therein).

After a potential cataclysmic variable system has been generated with the population synthesis code, the two detached components are given the opportunity to come into contact, via magnetic braking, within the age of the Galaxy (minus the CV formation time). However, the initial mass transfer may actually be unstable, thereby leading to a common envelope phase (and the ultimate demise of the binary system). As derived by RJW, the expression for the long-term mean mass transfer rate in a CV is given by $|\dot{M}|/M = N/D$, where the numerator, N, contains the drivers of mass transfer, e.g., systemic angular momentum losses, and the thermal expansion/contraction of the donor star (see eq. [33] in RVJ). The denominator is given by

$$D = \left[\left(\frac{5}{6} + \frac{\xi_{\rm ad}}{2}\right) - \frac{(1-\beta)q}{3(1+q)} - (1-\beta)\alpha(1+q) - \beta q\right], \tag{10}$$

where $q \equiv M_2/M_{\rm WD}$ (note that this is the inverse of the definition used in RVJ), β is the fraction of the mass lost by the donor star that is ultimately retained by the white dwarf, α is the specific angular momentum carried away by matter ejected from the binary system in units of the binary angular momentum per unit reduced mass, and $\xi_{\rm ad}$ is the adiabatic index of the donor star, i.e.,$[d\ln(R)/d\ln(M)]_{\rm ad}$ For our standard model (see Table 1), we take $\beta = 0$ (i.e., all the mass accreted by the white dwarf is eventually ejected in nova explosions[4]) and $\alpha = M_2^2/(M_2 + M_{\rm WD})^2$. With these definitions, the above equation reduces to

$$D = \frac{5}{6} + \frac{\xi_{\rm ad}}{2} - \frac{q(1+3q)}{3(1+q)}. \tag{11}$$

As discussed by RJW, stable mass transfer requires $N > 0$ and $D > 0$. As an example, consider donor stars with $M_2 < 0.3\ M_\odot$ and $\xi_{\rm ad} = -\frac{1}{3}$. In this case, stability (based on eq. [11]) requires that $M_2 < M_{\rm WD}$. This allows for considerably larger values of M_2 than the more conventional limit for conservative transfer, in which $M_2 < \frac{2}{3}M_{\rm WD}$ is required for stable mass transfer (with low-mass unevolved donors). Thus, the mass ratios that appear in our population synthesis can often approach unity or exceed it.

4.3. *Generating the Population Synthesis Tracks*

We define a birth rate function, BRF(t), for the progenitor primordial binaries, where t is the elapsed time between the formation of the Galaxy and the birth of the primordial binary. If a binary is born at time t, then an additional time $\tau_{\rm prim}$ must elapse before the primary evolves to the point where a common envelope phase may occur (see § 4.1). We define this time $(t + \tau_{\rm prim})$ to be the birth time of the incipient CV. The resultant zero-age CV is then evolved in the binary evolution code for a total time $t_{\rm max} = (10^{10} - \tau_{\rm prim})$ yr, which is the maximum time any CV that is descended from a similar primordial binary could evolve before the current epoch. (The binary evolution code starts with the white dwarf and companion star as they emerge from the common envelope, so the elapsed time, $t_{\rm ev}$, includes the interval before the donor star fills its Roche lobe.) At each step in the evolution code, specified by time $t_{\rm ev}$ (with respect to the first time step in the code), we sum in discrete binned arrays for various combinations of $P_{\rm orb}$, M_2, $M_{\rm WD}$, q, $\dot{M}$, $T_{\rm eff}$, and L_2, the following quantity, ΔQ:

$$\Delta Q = \frac{\Delta t \times {\rm BRF}(10^{10} - \tau_{\rm prim} - t_{\rm ev})}{N}. \tag{12}$$

In this expression, the argument of BRF is the time that the primordial binary was born with respect to the formation of the Galaxy, Δt is the time interval for that particular step in the evolution run, and N is the total number of systems that are selected to start the population synthesis run. For all of the population synthesis runs in this study, the BRF was taken to be constant in time. Even though we have adopted a constant stellar birth rate per unit time, the method we use for generating the CV population at the current epoch is completely general (see also Kolb 1993).

The net result of this procedure is that the sum of the ΔQs at the end of the population synthesis run, in any particular bin, represents the number of CVs at the current epoch with that particular parameter value.

5. POPULATION SYNTHESIS RESULTS

The computed population of current-epoch CVs as generated by the above techniques is displayed as a sequence of color images in Figures 3–7. In Figure 3 we show the model CV population in the $\dot{M}$-$P_{\rm orb}$ plane for our standard model

[4] See Schenker et al. (1998) for a justification as to why it is valid to approximate the ejection of mass in a series of nova explosions with a constant value of $\beta = 0$.

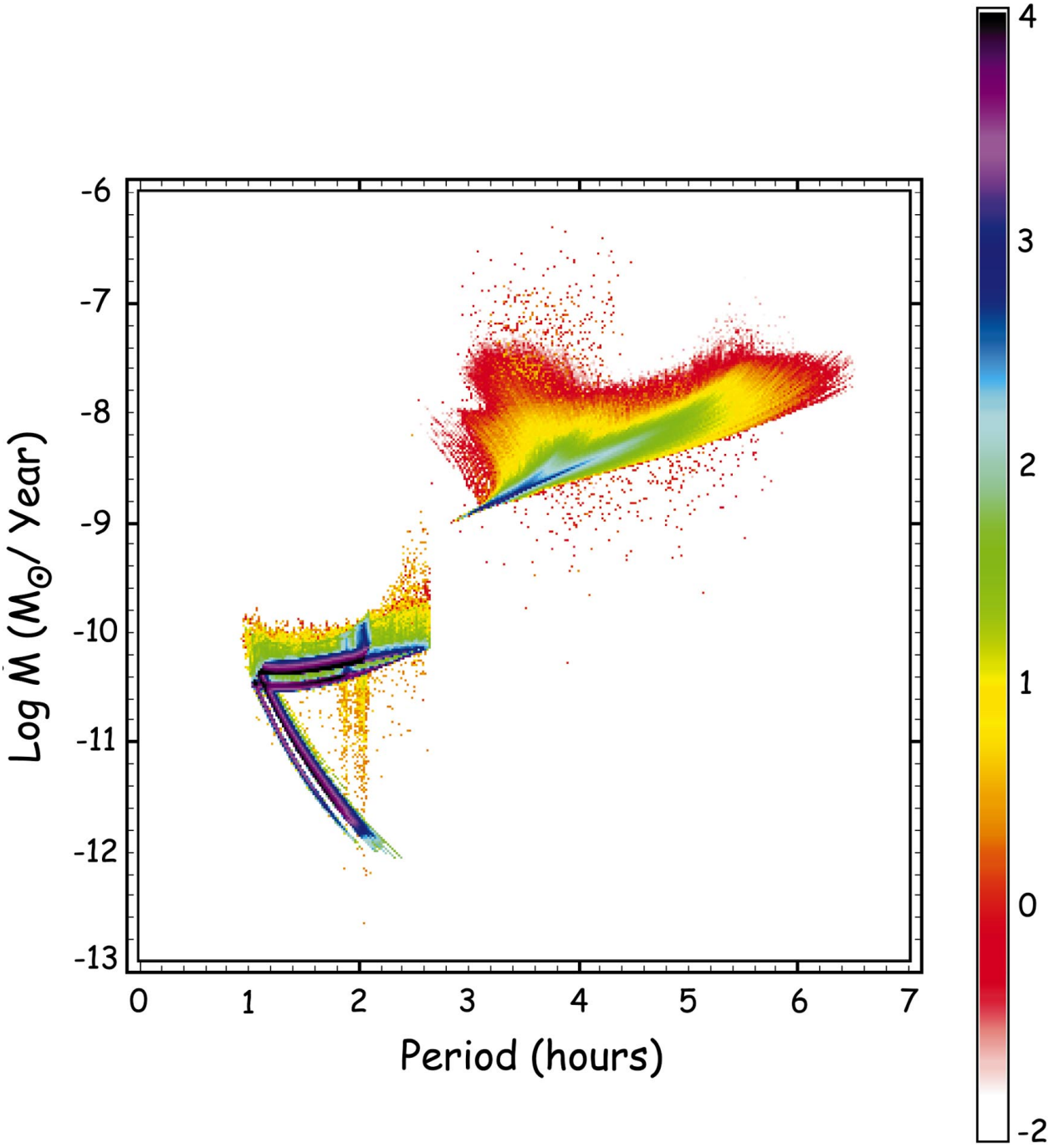

FIG. 3.—Computed population of cataclysmic variables at the current epoch in the $\dot{M}$-$P_{\rm orb}$ plane for our standard model (see Table 1). Here $\dot{M}$ is the mass transfer rate and $P_{\rm orb}$ is the orbital period. The color represents the logarithm of the number of systems in a particular $\dot{M}$-$P_{\rm orb}$ cell, of which there are 100 per hour interval in $P_{\rm orb}$ and 100 per decade in $\dot{M}$. The color scale is given on the right-hand side of the figure. We note that the scattered, isolated (*red*) points in the image *below* the main tracks are minor numerical artifacts of the evolution code that occasionally appear when the Roche lobe makes initial contact with the atmosphere of the donor star. One of these dots corresponds to only $\sim$0.1 CVs in the entire Galaxy at the current epoch, and so is of no significance.

(see also Fig. 2*a*). The image is generated in such a way that the color reflects the logarithm of the number of current-epoch CVs at a particular location in the $\dot{M}$-$P_{\rm orb}$ plane. In each of the images the color scale is located on the right-hand side. The image in Figure 3 is composed of 100 pixels hr^{-1} intervals in $P_{\rm orb}$ and 100 pixels per decade in $\dot{M}$.

The most noteworthy features in Figure 3 include the distinct groups of systems located above and below the period gap. Note the substantial difference in $\dot{M}$ for systems above and below the period gap; for the latter systems only gravitational radiation losses drive mass transfer. The minimum orbital period ($P_{\rm min} \sim 65$ min) is also clearly evident, as are systems that have evolved well past the minimum period back up to values of $P_{\rm orb} \sim 2$ hr. It has been proposed that these latter systems may be related to the so-called TOADs ("tremendous outburst amplitude dwarf novae"; see, e.g., Howell et al. 1995, HRP). In the systems above the gap, there is a central band of evolutionary tracks (*blue* and *green*) where a typical CV is most likely to be found at a particular point in time during its evolu-

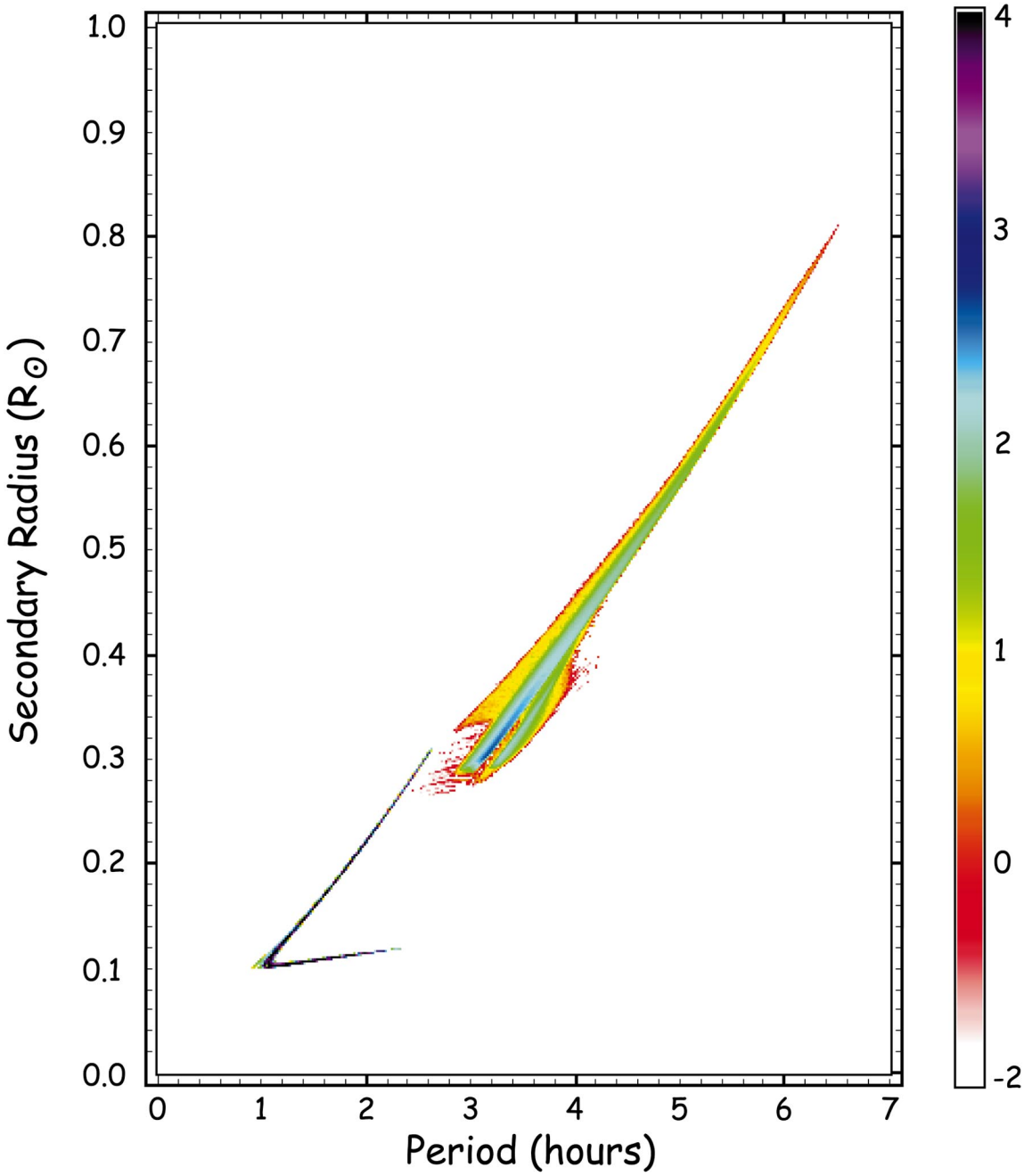

FIG. 4.—Computed population of cataclysmic variables at the current epoch in the R_2-P_{orb} plane for our standard model (see Table 1). Here R_2 is the radius of the donor star. The color represents the logarithm of the number of systems in a particular R_2-P_{orb} cell, of which there are 100 per 0.1 $R_\odot$ and 100 per hour interval in P_{orb}. The color scale is given on the right-hand side of the figure.

tion. One also notices very short lived episodes (*red* and *yellow*) of high mass transfer rates. These occur for individual systems as the donor star first fills its Roche lobe and commences mass transfer, but before it can come into a quasi-steady state of mass transfer (see discussion in § 2). The same type of behavior is seen (*green structure*) for systems that have come into contact for the first time below the period gap, i.e., with initially very low mass donor stars. The two main tracks (*purple*) evident in the systems below the period gap are for He (lower) and CO (upper) white dwarfs, respectively. We also call attention to the small vertical (*blue*) feature at $P_{orb} \sim 2$ hr. This may be related to the statistically significant larger number of CVs with periods in the range of 110–120 minutes (first pointed out by Hameury et al. 1988b). Finally, we note that there are systems found within the period gap, though fewer per period interval than for systems below the gap. Systems found within the period gap are typically ones that had initial donor masses of $\sim$0.22–0.34 $M_\odot$ and commenced Roche lobe overflow at orbital periods in the range of $\sim$2–3 hr (see also Fig. 2 and its associated discussion).

Further, in regard to the $\dot{M}$-P_{orb} plane shown in Figure 3, we point out that for systems above the period gap, the width of the distribution in $\dot{M}$ at any fixed value of P_{orb} is

only about a factor of ~ 2 (we define the "width" as containing $\sim 80\%$ of the systems). This is in contrast with the *observed* spread in $\dot{M}$ for CVs, which is closer to an order of magnitude (see, e.g., Patterson 1984; Warner 1995). One cause of this spread may be the inherent uncertainty in translating observed parameters into accurate estimates of $\dot{M}$. Additionally, some of this discrepancy might be resolved by the inclusion of the effects of nova explosions in CVs which, on a quasi-regular basis, slightly increase (or perhaps even decrease) the orbital separation (e.g., by $\delta a/a \sim 10^{-4}$), which is sufficient to change $\dot{M}$ appreciably for some interval of time (see Shara et al. 1986; Schenker et al. 1998; U. Kolb et al. 2001, in preparation). However, we note that Schenker et al. (1998) showed that, except for extreme model parameters, the occurrence of the nova explosions generally does not substantially affect the overall secular evolution of the CVs. Therefore the main results and conclusions presented in this work should be robust even without the inclusion of *orbital* perturbations due to nova explosions (we do, in fact, take into account the mass and angular momentum lost in such events).

The population of current-epoch CVs in the R_2-$P_{\rm orb}$ plane for our standard model is shown in Figure 4. The shape traced out in this figure represents a statistical ensem-

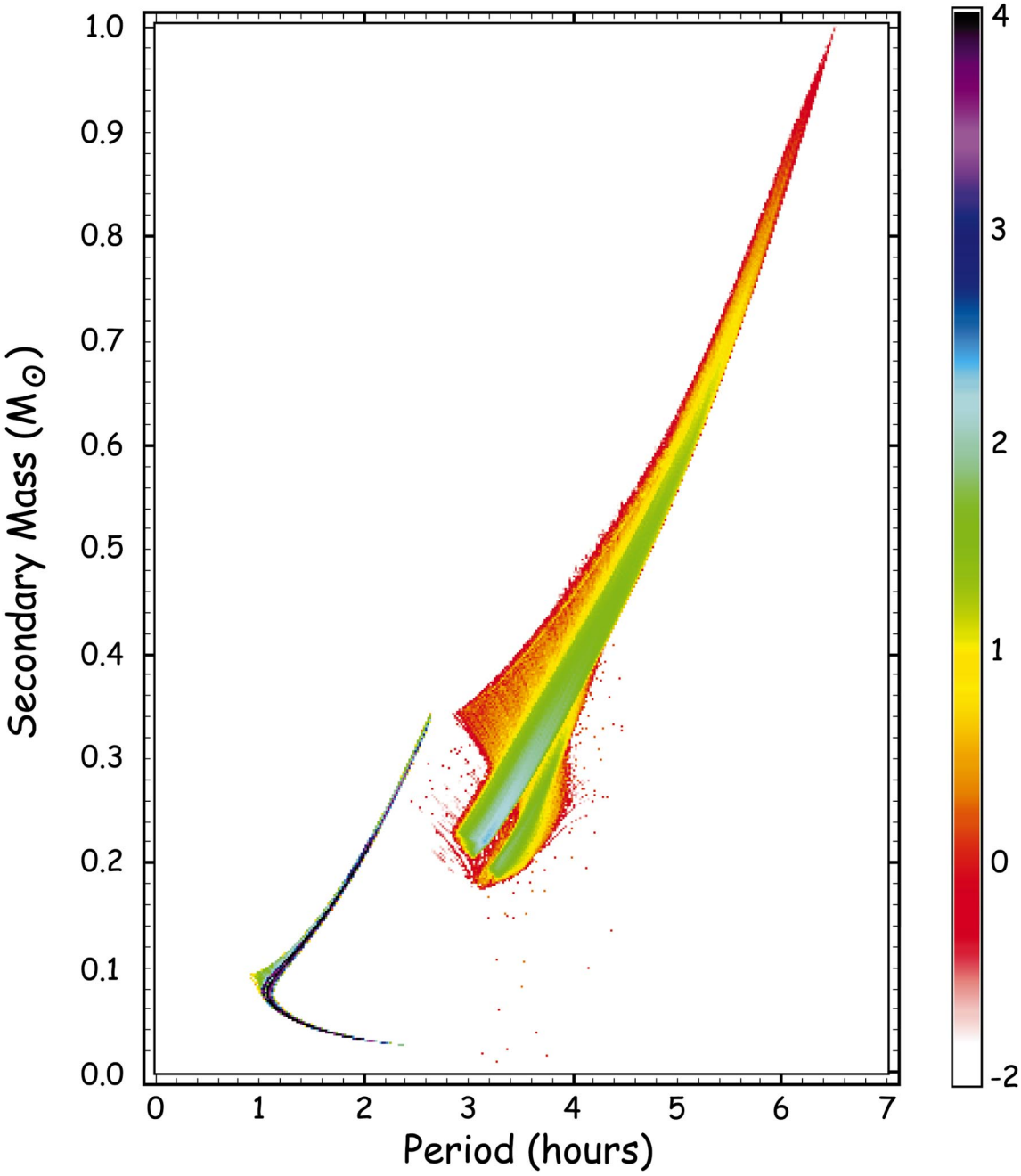

FIG. 5.—Computed population of cataclysmic variables at the current epoch in the M_2-$P_{\rm orb}$ plane for our standard model (see Table 1). Here M_2 is the mass of the donor star. The color represents the logarithm of the number of systems in a particular M_2-$P_{\rm orb}$ cell, of which there are 100 per 0.1 $M_\odot$ and 100 hr^{-1} interval in $P_{\rm orb}$. The color scale is given on the right-hand side of the figure.

ble of the type of evolutions graphed in Figures 2*c* and 2*f*. The usual features of the "upper branch" of systems above the period gap, systems in the "lower branch" below the gap, and the minimum orbital period are all represented in this figure. Again, as in Figure 3, we see that some systems are formed within the period gap. It is difficult from this image to judge quantitatively how many systems are in the gap, versus the density of points just below the gap. This is quantified later in this section (see Fig. 9). Note that an extrapolation of the "upper branch" to shorter orbital periods would undershoot the "lower branch," on which the stars are close to thermal equilibrium. As discussed in § 2, this undershooting actually (counterintuitively) results from the thermal *bloating* of the donor star when it has a higher mass loss rate that is driven by magnetic braking. In particular, see equation (7), in which we show that R_2 scales as $f^{-0.65}$, where f is the bloating factor. The low-density features (*yellow*) just above the main tracks through the "upper branch" are systems that have just come into Roche lobe contact for the first time and have not yet established a quasi-steady state of mass transfer. The blue-green "thumb" feature just below the main track of the "upper branch" near the top edge of the period gap represents systems with He white dwarfs and donor stars of comparable mass that have just come into contact. Their mass transfer rates are higher than normal for these orbital periods; thus the bloating factors for these donor stars are significantly larger than for systems on the main track (see also Fig. 2*f*).

Perhaps the most dramatic demonstration of the effects of thermal bloating of the donor star can be seen in Figure 5, which shows the population of current-epoch CVs in the M_2-$P_{\rm orb}$ plane for our standard model. The shape traced out in this figure represents a statistical ensemble of the type of evolutions graphed in Figures 2*b* and 2*e*. All of the features that appear in the R_2-$P_{\rm orb}$ image (Fig. 4) also appear in this M_2-$P_{\rm orb}$ image, except in a more exaggerated form. This is a direct result of the simple scaling argument summarized in equation (6) in § 2, which indicates that the bloating effect on the masses just above the period gap scales as $M_2 \propto f^{-1.95}$. A casual inspection of Figure 5 shows that the masses of the donor stars in CVs with periods just above the period gap are fully $\sim$40% lower than would be expected if their radius-mass relation followed that of main-sequence stars. It is this effect that we propose be used to discriminate between the currently held explanation for the period gap and alternate scenarios. We return to a quantitative discussion of this issue in the next section.

Lastly, in regard to the color images of the R_2-$P_{\rm orb}$ and M_2-$P_{\rm orb}$ planes (Figs. 4 and 5), we comment on the relatively large spreads in R_2 and M_2 for systems above the period gap in contrast with those below the gap. As we showed in equations (6) and (7), for a fixed value of the bloating parameter f, both M_2 and R_2 are unique functions of the orbital period (which would imply narrow tracks). For systems well above the period gap, the Kelvin timescale, $\tau_{\rm KH}$, is shorter than the mass-loss timescale, $\tau_{\dot{M}} \equiv M/\dot{M}$, but, as the orbital period decreases and approaches the period gap, the two timescales become more comparable. Thus, as discussed in § 2, the donor star must become ever more bloated so as to establish a luminosity deficit, which in turn enables the donor to contract inside its ever shrinking Roche lobe. Additionally, the adiabatic stellar index is changing from positive to negative, and this tends to make the star expand even further as it loses mass (see also Beuermann et al. 1998). These two effects lead to the bloating behavior that is seen in Figures 4 and 5. The actual amount of bloating depends upon the absolute values of the two constituent masses as well as on the thermal history of the donor; therefore, it is to be expected that f may vary from one donor star to another. As a result, we see not only enhanced bloating as systems approach the period gap, but a relatively wider and wider spread in the values of M_2 and R_2 for these systems, especially for $P_{\rm orb}$ in the range of 3–5 hr. By contrast, for systems just below the period gap, $\tau_{\dot{M}}$ increases abruptly—by about an order of magnitude—because the mass transfer is then driven only by gravitational radiation losses (at least according to our model), and therefore the donor stars can remain much closer to thermal equilibrium. This allows the systems right below the gap to establish a nearly main-sequence radius-mass relation (i.e., $f \simeq 1$), thereby leading to a relatively narrow set of evolution tracks. However, as the secondary's mass approaches the minimum main-sequence mass (before the orbital period minimum), $\tau_{\rm KH}$ becomes very long (because of a sharp decrease in the secondary's nuclear luminosity), thereby causing $\tau_{\rm KH}$ and $\tau_{\dot{M}}$ to again become approximately equal. Thus, the width of the tracks broadens somewhat near the orbital period minimum. For systems beyond the orbital period minimum, the interiors become increasingly electron degenerate. This leads to a nearly unique mass-radius relationship $R_2 \propto M_2^{-1/3}$, which, in turn, leads to entirely different $R_2(P_{\rm orb})$ and $M_2(P_{\rm orb})$ relations than are given by equations (6) and (7). Nonetheless, they are unique relations (easily derivable from eqs. [4] and [5]), which also lead to a very narrow set of tracks in Figures 4 and 5.

The distribution of expected mass ratios, q, in CVs at the current epoch is shown as a function of orbital period in Figure 6. At any given orbital period the range of q-values is considerably broader than the distribution of values of R_2 or M_2, as can be seen by comparison with Figures 4 and 5. The reason for this is straightforward. Equations (6) and (7) indicate that, as long as the bloating factor f depends largely on the orbital period of a CV, then both the radius and mass are nearly unique functions of the orbital period. Thus, the much broader distribution of q in Figure 6 is due largely to the substantial range of masses that the white dwarf may have, which is much less constrained by the orbital period than is M_2. For both the systems above and below the period gap, the upper set of tracks corresponds to He white dwarfs, while the lower tracks are for CO white dwarfs. The period gap is especially conspicuous in this figure, especially for systems with CO white dwarfs. Note that some of the mass ratios extend up to values of unity and, in some cases, above unity. The stability of mass transfer in these systems was discussed in § 4.2 (see eq. [11]).

The evolution of our model population of CVs in the $T_{\rm eff}$-$P_{\rm orb}$ and luminosity-$P_{\rm orb}$ planes is shown in Figure 7. The left-hand panel displays the effective temperature, $T_{\rm eff}$, of the donor star, while the right-hand panel has a superposition of the optical (bolometric) luminosity, $L_{\rm opt}$, and nuclear luminosity, $L_{\rm nuc}$. Where the two sets of luminosity tracks cross (e.g., near $P_{\rm orb} = 1$ hr) or overlap (e.g., to a minor extent between 3 and 6 hr), the default is to display $L_{\rm opt}$. With regard to the $T_{\rm eff}$ curves, we first note that the absolute temperature scale for our main-sequence stars (based on our bipolytrope code) is somewhat shifted from that produced with more sophisticated codes, e.g., our

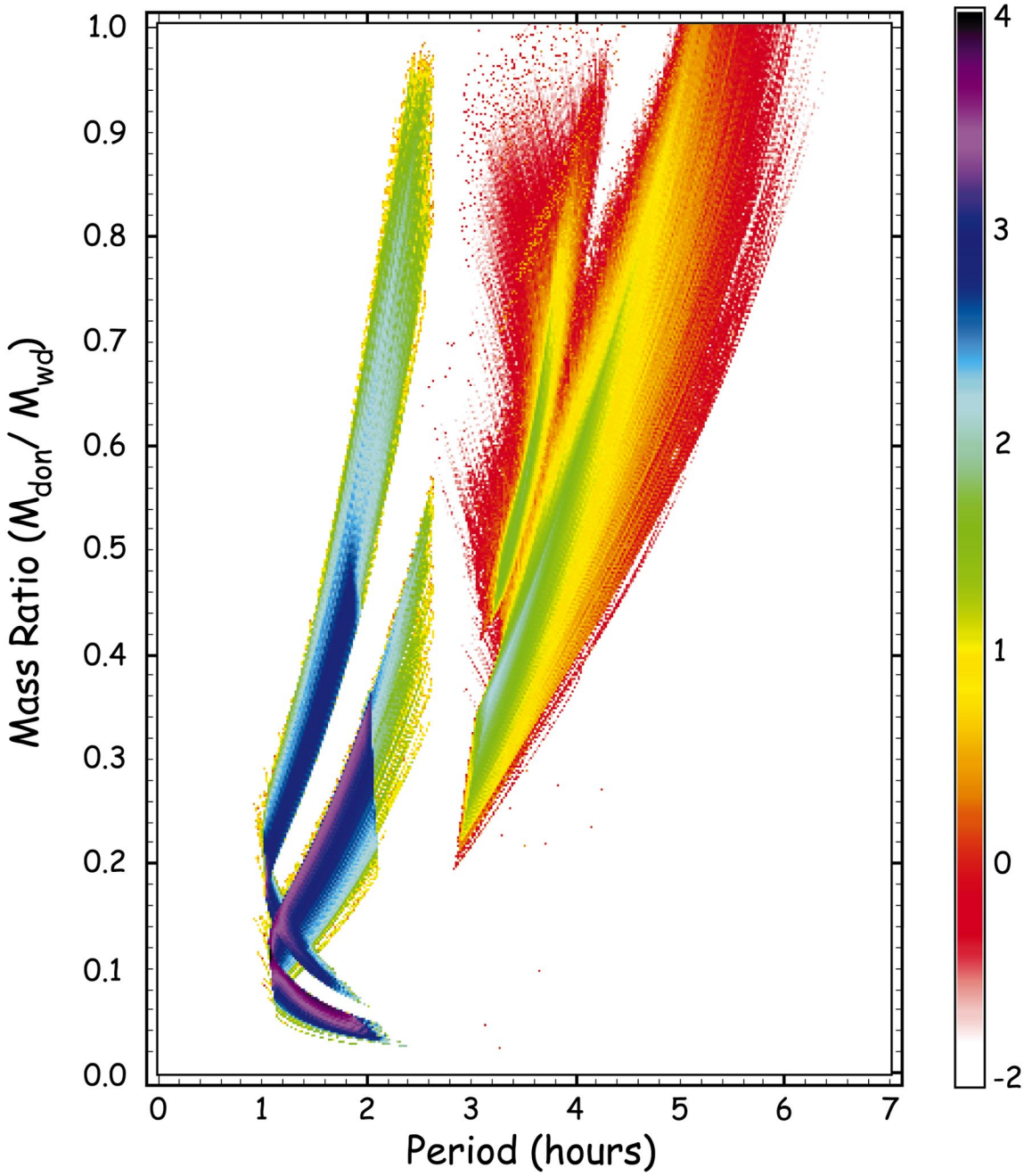

FIG. 6.—Computed population of cataclysmic variables at the current epoch in the q-P_{orb} plane for our standard model (see Table 1); $q \equiv M_2/M_{WD}$. The color represents the logarithm of the number of systems in a particular q-P_{orb} cell, of which there are 100 per $\Delta q = 0.1$ and 100 per hour interval in P_{orb}. The color scale is given on the right-hand side of the figure.

bipolytrope main-sequence models are $\sim$200 K higher than the DNC models over the mass range of 0.85–0.1 $M_\odot$. However, aside from this small quantitative difference we are confident that the overall qualitative trends and shapes of these tracks are highly indicative of the behavior and properties of the donor through its evolutionary history. Note that for values of P_{orb} below the gap as well as above $\sim$5 hr, the T_{eff} tracks are quite narrow, in analogy with the tracks in the M_2-P_{orb} and R_2-P_{orb} planes, since the donor stars are typically quite close to thermal equilibrium. By contrast, within the period range of 3–5 hr, T_{eff} of the donors is systematically lowered by up to 250 K compared with T_{eff} of main-sequence stars at the same P_{orb}. This lower temperature amounts to a change to a later spectral type (at a given P_{orb}) of $\sim$2–4 in decimal subclass. Additionally, we can see from Figure 7 that, over this same period range, the use of temperature (or spectral type) to determine the mass of the secondary star would require very precise measurements, since the expected T_{eff}-P_{orb} distribution is relatively flat. We draw two conclusions from this figure: (1) an observationally produced T_{eff}-P_{orb} or spectral type–P_{orb} relation for CVs should indeed yield a fairly simple shape (especially when smoothed out by uncertainties in the measurements) and (2) the use of T_{eff} or spectral type in the 3–5 hr period

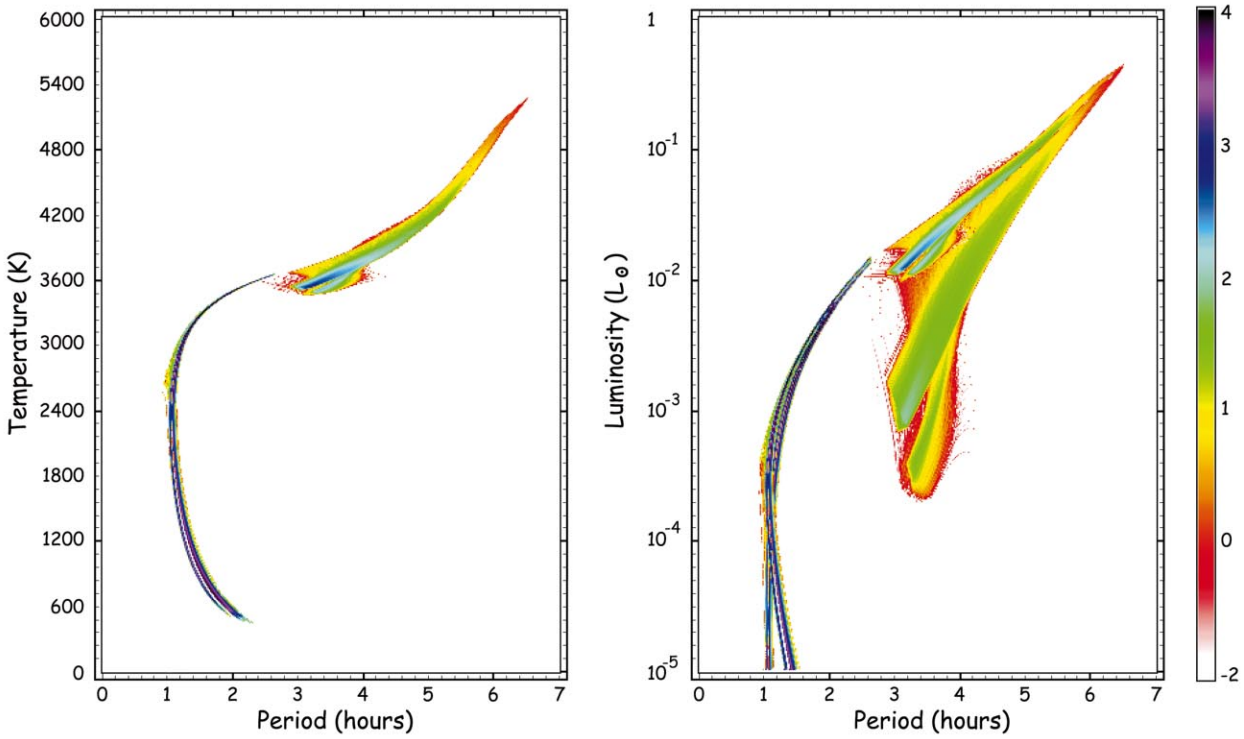

FIG. 7.—Computed population of cataclysmic variables at the current epoch in the $T_{\rm eff}$ /$P_{\rm orb}$ plane (*left panel*) and the luminosity-$P_{\rm orb}$ plane (*right panel*) for our standard model (see Table 1). We show both the stellar luminosity (*top curve*) and the core nuclear luminosity (*lower distributions*). The color represents the logarithm of the number of systems in a particular L-$P_{\rm orb}$ or $T_{\rm eff}$-$P_{\rm orb}$ cell, of which there are 100 per decade in L, 100 per 500 K in $T_{\rm eff}$, and 100 per hour interval in $P_{\rm orb}$. The color scale for both plots is given on the right-hand side of the figure.

range will not yield reliable indications of the mass of the donor star.

Recently, Smith & Dhillon (1988)[5] published results that took a critical look at the relation between orbital period, spectral type, and secondary mass based on the best observational data available in the literature. They presented a relatively smooth spectral type–orbital period relation but concluded that one cannot reliably estimate M_2 in any given CV based solely on its spectral type. Our theoretical results are quite consistent with their conclusion.

The image in the right-hand panel of Figure 7 displays a superposition of the evolutionary tracks for $L_{\rm opt}$ and $L_{\rm nuc}$ as functions of $P_{\rm orb}$. For systems above the gap, the highest luminosity track corresponds to $L_{\rm opt}$, while the two prominent lower (*green*) tracks are for $L_{\rm nuc}$ and are related to the corresponding features in the M_2-$P_{\rm orb}$ image. These two lower luminosity tracks are for systems with CO (upper) and He (lower) white dwarf accretors (see the discussion of Fig. 5). The large luminosity deficit in the $P_{\rm orb}$ range of 3–5 hr, already discussed in § 2, shows up quite dramatically in this Figure 7. The group of systems with the highest luminosity deficit (with He white dwarf accretors) has the largest values of $\dot{M}$ and the donors are the most out of thermal equilibrium (largest bloating factor). In spite of the relatively low values of $L_{\rm nuc}$ in this period range, the bolometric luminosity $L_{\rm opt}$ is depressed only modestly (e.g., by factors of $\lesssim 2$) over main-sequence stars at the same orbital period. For systems below the period gap, both luminosities fall off dramatically, especially for donor masses below ~ 0.05–0.08 $M_\odot$, where the donors are already below the hydrogen-burning main sequence, and are cooling toward their ultimate degenerate state. The higher track for all points below the period gap corresponds to $L_{\rm opt}$, the lower one to $L_{\rm nuc}$. While it is formally true that the $L_{\rm opt}$ and $L_{\rm nuc}$ tracks "cross" at $\sim 10^{-4}\ L_\odot$, the two luminosities are never equal in this part of the diagram; they reach the crossing point at very different times.

Finally, with regard to the color image representations of CV populations in parameter space, we note that in Figures 3–7, the color represents the logarithm of the numbers of systems expected at the current epoch. As can be seen in any of these figures (but especially Figs. 3 and 6), the number of systems below the period gap outweighs the number above the period gap by a large margin (by about 100:1; see the more quantitative discussion below; see also de Kool 1992, Kolb 1993). However, because of observational selection effects, the systems with the shorter orbital periods, lower values of $\dot{M}$, and generally longer intervals between dwarf-nova outbursts, are more difficult to discover. The exact factors that go into the observational selection effects are complex, especially since some CVs are discovered via their dwarf-nova outbursts, others (e.g., longer period CVs) by their blue colors or flickering behavior, and still others by their nova outbursts. Some of these issues are discussed in RJW and Kolb (1993). For purposes of the present work we will indicate only qualitatively how the numbers of observationally known CVs might be expected to be distributed by orbital period. We adopt two crude detectability factors which scale simply as $\dot{M}^{3/2}$ and as $\dot{M}$. The first of these is

[5] The sample used in Smith & Dhillon consisted of what are believed to be 55 reliable spectral types and 14 reliable secondary star masses. All systems in their sample have $P_{\rm orb} > 90$ minutes and $V_{\rm min}$ brighter than ~ 17 mag, thus Smith & Dhillon's conclusions about finding no evidence for post–period minimum systems or very low mass brown dwarf-like secondaries cannot be drawn from the sample they used.

appropriate to steady state accretion luminosities that are proportional to $\dot{M}$ in the optical bandpass, which give rise to a bolometrically flux-limited detectability proportional to $\dot{M}^{3/2}$ (analogous to the 3/2 slope of a log (N)– log (S) curve for isotropically distributed sources). The other scaling, appropriate to the case in which the flux in the optical bandpass is proportional to $\dot{M}^{2/3}$ (see Lynden-Bell & Pringle 1974; RJW; Webbink et al. 1987), leads to a flux-limited detectability proportional to $\dot{M}$. Other factors leading to the discovery of CVs, beyond the simple consideration of flux limited samples, in particular the detection of dwarf nova outbursts, would undoubtedly substantially modify the rudimentary dependences on $\dot{M}$ that we use here for purposes of illustration. In Figure 8 we redisplay Figure 3, but this time rescaled by a factor of $\dot{M}$. It is clear from a casual inspection of Figure 8 that the number of "detectable" systems above the period gap is now at least as great as for those below the gap. The actual quantitative values for this simple scaling are presented below. We again caution, however, that either an $\dot{M}^{3/2}$ or $\dot{M}$ scaling is oversimplified.

The color images of parameter space shown in Figures 3–7 can be displayed in a somewhat more quantitative fashion by projecting the numbers of systems onto the various axes and plotting the results as simple histograms. For example, the data used to produce any of the images can be projected onto the $P_{\rm orb}$ axis to yield the orbital period distribution. The results are shown in Figure 9. The solid histogram in Figure 9*a* is the distribution of CVs at the current epoch in the entire Galaxy for our standard

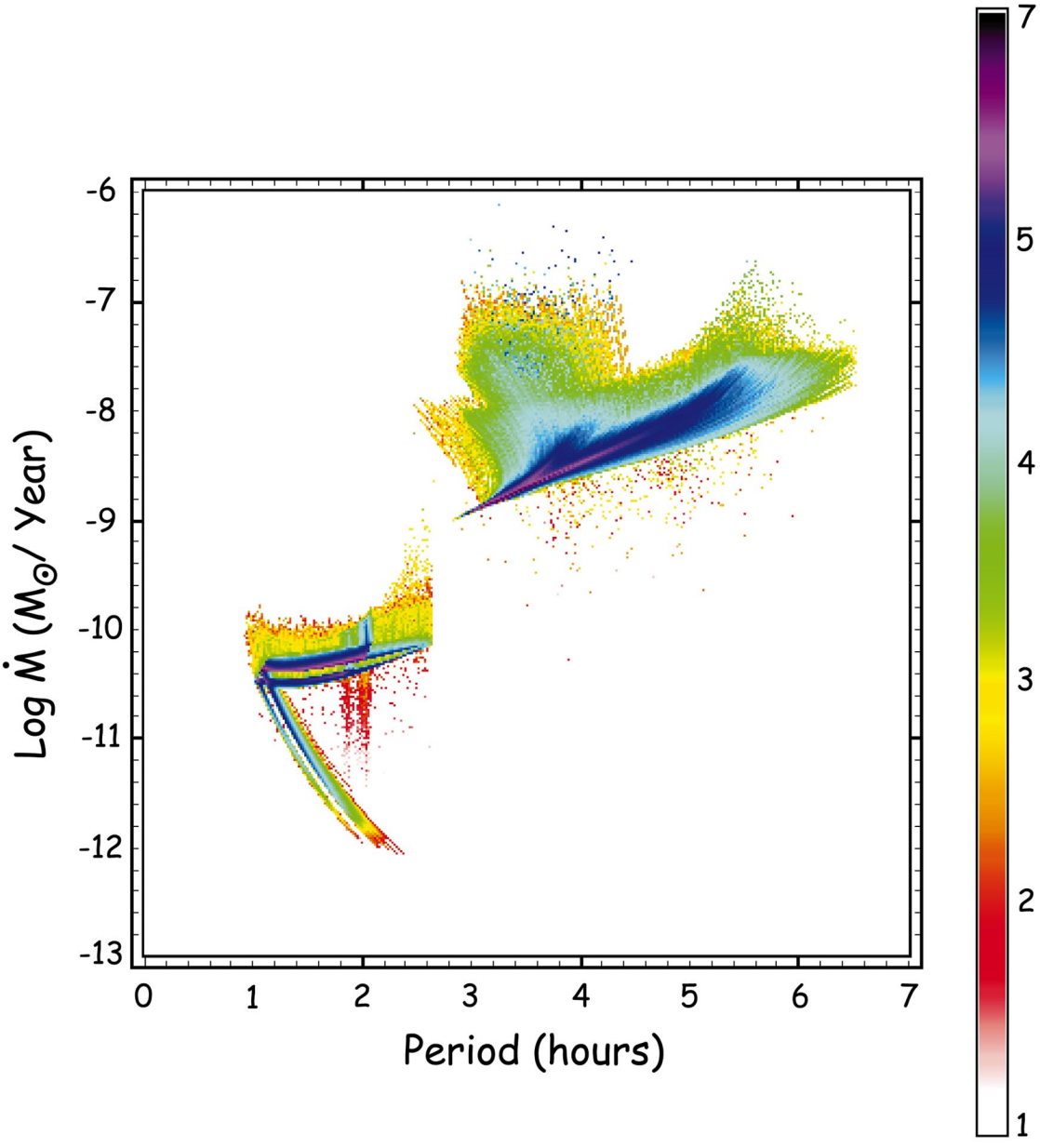

FIG. 8.—Same as Fig. 3, except that the population has been scaled by $\dot{M}^1$ to crudely take into account observational selection effects

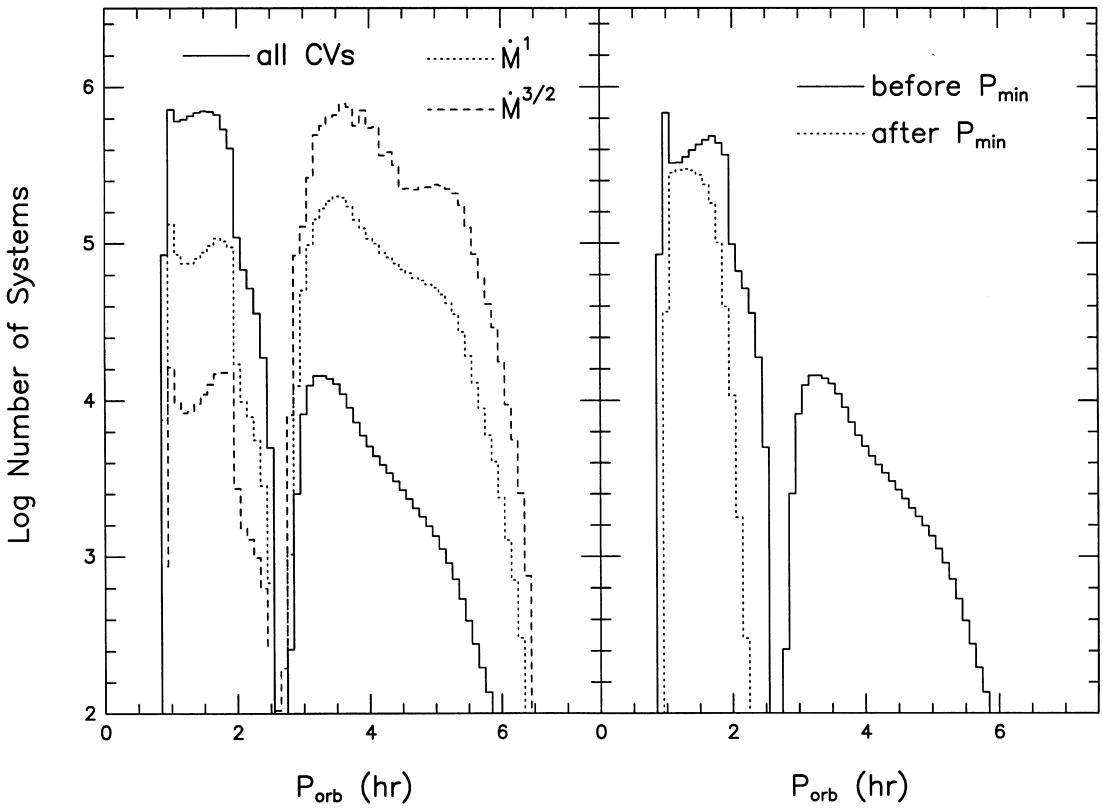

FIG. 9.—Computed orbital period distributions for cataclysmic variables at the current epoch. *Left panel:* the solid curve is the distribution for all systems that appear in Fig. 3; the dashed curve was produced by scaling the contributions of each system evolved by $\dot{M}^{3/2}$, while the dotted curve is for an $\dot{M}^1$ scaling (see text). The $\dot{M}^{3/2}$- and $\dot{M}^1$-scaled curves have been shifted vertically by arbitrary amounts for ease in comparison. *Right panel:* the solid curve is for all systems in Fig. 3 that have not yet reached orbital period minimum; the dashed curve is for systems that have evolved past the orbital period minimum.

model (see Table 1). The stellar birthrate function and IMF in our standard model (eq. [8]) are normalized in such a way that there are ~ 0.6 stars born in the Galaxy per year with a mass greater than 0.8 $M_\odot$, just above the threshold for producing a remnant white dwarf by the current epoch. Thus, the "absolute values" of the numbers plotted in Figure 9 can be appropriately scaled up or down for either lower or higher assumed birthrates.

If the numbers of CV systems are scaled by the types of "observability factors" discussed above, before the histogram is produced, the results are the dashed and dotted histograms superposed in Figure 9*a*. As discussed above, in conjunction with Figure 8, this qualitatively helps to explain the relative numbers of CVs observed above the period gap compared with the number observed below (see especially the dotted histogram). Inspection of the compilation of CVs with known orbital periods given in Warner (1995) reveals that our histogram shown in Figure 9*a* with the $\dot{M}$ scaling provides qualitative agreement with current observational results, especially considering the many observational selection effects that exist (e.g., magnitude-limited color surveys, large-amplitude but infrequent outbursts compared with semiperiodic lower amplitude outbursts, discovery in X-ray surveys, etc.). The distributions of orbital period shown in Figure 9*b* are for systems that have not yet evolved to the minimum orbital period (*solid curve*) and systems that have evolved beyond the period minimum (*dashed curve*)—no scaling in $\dot{M}$ has been applied here.

The distributions of white dwarf masses and donor masses at the current epoch are shown in Figure 10 (left- and right-hand panels, respectively) for four different ranges of orbital period. The He and CO white dwarfs are easy to distinguish by mass. Note that for systems with $P_{orb} > 4$ hr, which typically have donor stars with masses greater than 0.4 $M_\odot$, there are few He white dwarfs, since the mass transfer would tend to be unstable. The distributions of donor star masses show a steady trend toward higher masses at the longer periods, as expected. This results qualitatively from the fact that the larger orbital periods require less dense, and therefore usually more massive, stars. Note that the distributions shown in this figure are not produced with sufficient resolution in P_{orb} to allow one to make quantitative predictions as to what mass donors are needed to validate the basic paradigm for the period gap. Such information may be found, however, in Figures 5 and 12 and Table 2.

The distribution of mass ratios q ($\equiv M_2/M_{WD}$) is shown in Figure 11 for two different orbital period ranges. Attempts to determine q observationally can be made from, for example, superhump period analysis or spectroscopic analysis. The observational distribution for q in short-period ($P_{orb} < 2$ hr) CVs has recently been compiled (Mennickent, Matsumoto, & Arenas 1999) and is seen to show an approximate Gaussian distribution with $\langle q \rangle = 0.14$. However, observational selection effects allow few CVs with small q to be discovered owing to their intrinsic faintness. Our results (Fig. 11, *top panel*) show that the actual distribution should not drop off at q values lower then 0.14, but rather should peak at values of $q = 0.05$–0.1, with an overall distribution that is clearly non-Gaussian. Discovery and observation of additional faint (short-period)

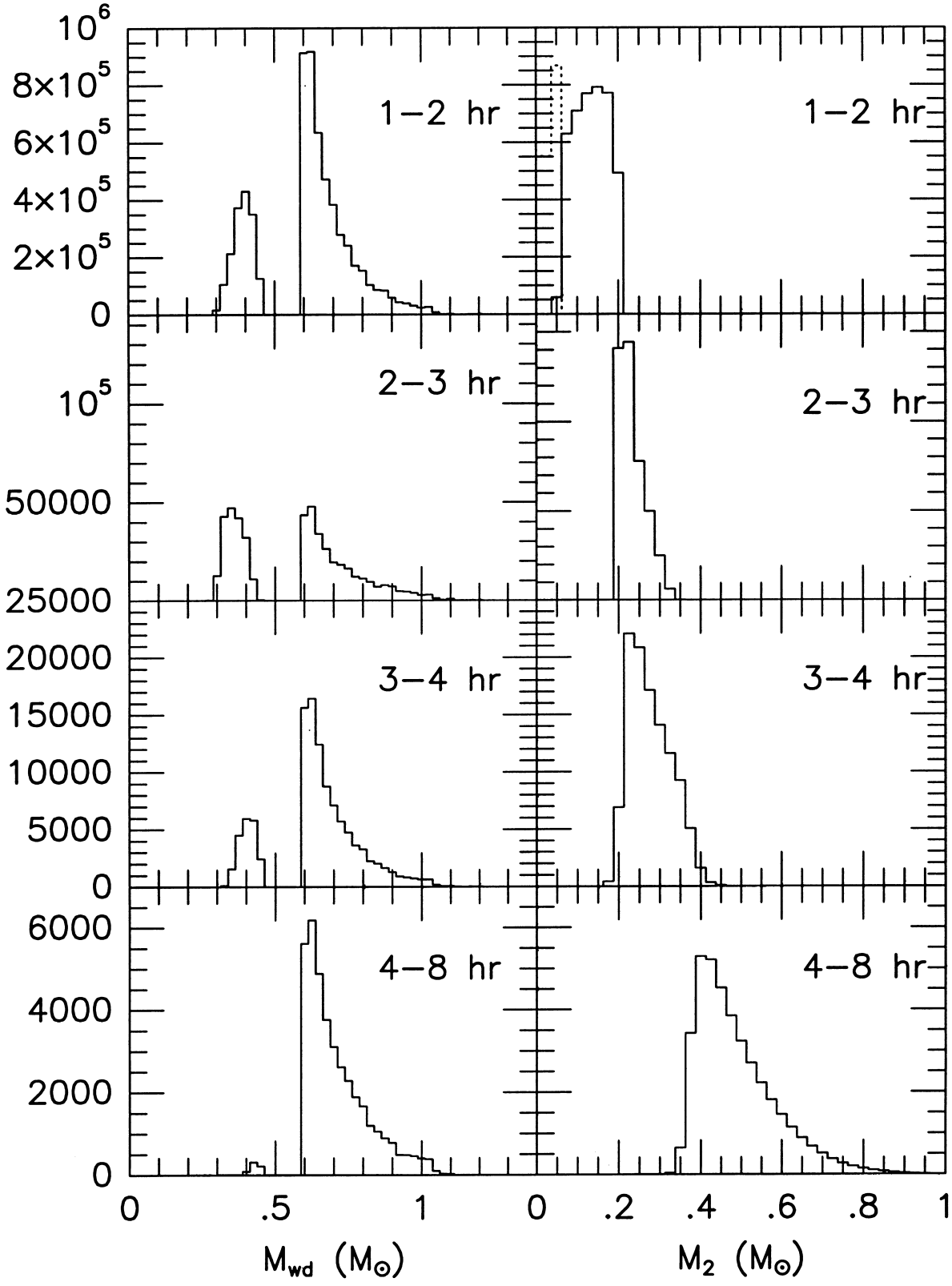

FIG. 10.—Computed distributions of the secondary (*right-hand panels*) and white dwarf masses (*left-hand panels*) in cataclysmic variables at the current epoch. The mass distributions are ordered according to the range of orbital period. The dotted histogram (*upper right*) is for post–period minimum CVs and has been arbitrarily divided by 1.5 for presentation purposes.

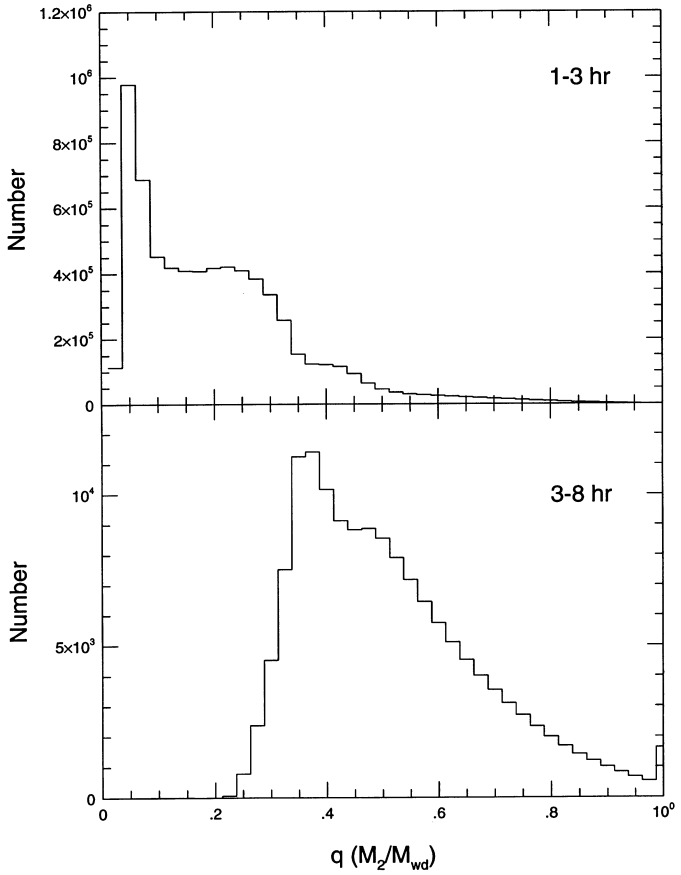

FIG. 11.—Computed distribution of mass ratios in cataclysmic variables at the current epoch. The top panel is for systems with orbital periods in the range of 1–3 hr (which includes all post–period-gap systems), while the bottom panel is for systems above the period gap.

CVs are needed in order to confirm this theoretical prediction.

6. TEST OF THE BASIC PARADIGM

The rapid rate of mass loss for donor stars in CVs just above the period gap should lead to significant thermal bloating of the donor. Thus, in the conventional paradigm for the formation of the period gap, this mass-loss rate is abruptly decreased at orbital periods near 3 hr and the donor star shrinks inside its Roche lobe (see § 2), leading to the cessation of mass transfer. Specific choices of the parameters utilized in any such evolutionary model change the bloating factor quantitatively but do not change the overall evolution qualitatively. To demonstrate this, we show in Figure 12 CVs at the current epoch in the M_2-$P_{\rm orb}$ plane for four different sets of model parameters (see Table 1). Figure 12*a* is for our standard model, while the other panels are for models where (Fig. 4*b*) the proportionality constant in the magnetic braking formula was reduced by a factor of 2 ($C_{\rm MB} = \frac{1}{2}$), (Fig. 4*c*) the specific angular momentum carried away by mass lost from the system in nova explosions is twice that of the white dwarf ($\alpha = 2\alpha_{\rm WD}$), and (Fig. 4*d*) all mass transferred to the white dwarf is ultimately retained by the white dwarf (i.e., $\beta = 1$; in this somewhat artificial model, white dwarfs are allowed to exceed the Chandrasekhar limit).

We see from a study of Figure 12 that the effects of thermal bloating on the mass of the donor stars in CVs for orbital periods just above the gap are qualitatively similar for all four models. The actual factors by which the masses are lower than would be inferred by making the assumption that the donor has a main-sequence mass-radius relation range from 25%–50%; the exact range depends on which model parameters are chosen and whether one includes the CVs with He white dwarfs where the mass transfer can be only marginally stable. To quantify the effect of thermal bloating on mass determinations, we have carried out weighted least-squares fits of polynomials to each of the "upper branches" shown in Figure 12. The results are given in Table 2, which also includes the evaluation of the polynomial fit at $P_{\rm orb} = 3$ hr. As we can see from Table 2, the effect of thermal bloating on the inferred donor mass of CVs is quite significant, and potentially testable, for any of these models.

We note that, in general, the *spread* in values of M_2, at a given $P_{\rm orb}$, around the best-fit $M_2(P_{\rm orb})$ curve is substantially smaller than the mean deviation from an $M_2(P_{\rm orb})$ curve based on the assumption of a main-sequence mass-radius relation, especially in the crucial period range of 3–5 hr. A large part of this spread is due to the different values of the mass of the accretor, M_1, with lower values of M_2 corresponding to the lower values of M_1 (see also the discussion in § 5). However, we do not attempt here to produce fits of the more general form $M_2(P_{\rm orb}, M_1)$. Such fits are not straightforward to construct since, among other things, there is the added complication of the existence of a minimum value for M_1 at any $P_{\rm orb}$ (due to issues of mass transfer stability; see § 4.2). In any case, the main effect to be confirmed observationally concerns the substantially reduced values of M_2 just above the period gap (3–5 hr), compared to what would be expected if the donor stars followed a main-sequence mass-radius relation. If sufficient numbers of high-quality mass determinations of the secondary stars can be made, and if this basic effect is confirmed, then a secondary goal would be to look for a weak, but positive, correlation between M_2 and M_1.

TABLE 2

SUMMARY OF POLYNOMIAL FITS TO M_2-$P_{\rm orb}$ RELATIONS[a]

Model[b]	c_0	c_1	c_2	c_3	$M_2(P_{\rm orb} = 3$ hr)[c]
A. Standard model	0.005863	−0.001251	0.02353	0.0	0.214
B. Reduced magnetic braking	−0.4323	0.3294	−0.04942	0.005028	0.247
C. High angular momentum losses	−0.1829	0.1031	0.01041	0.0	0.220
D. Conservative mass transfer	−0.5280	0.3856	−0.06261	0.006076	0.230
Main-sequence donor	...	...	...	...	0.35

[a] For systems with $P_{\rm orb} > 3$ hr. Fits are of the form $M_2 = c_0 + c_1 P_{\rm orb} + c_2 P_{\rm orb}^2 + c_3 P_{\rm orb}^3$.
[b] Models are defined in Table 1.
[c] In units of $M_\odot$.

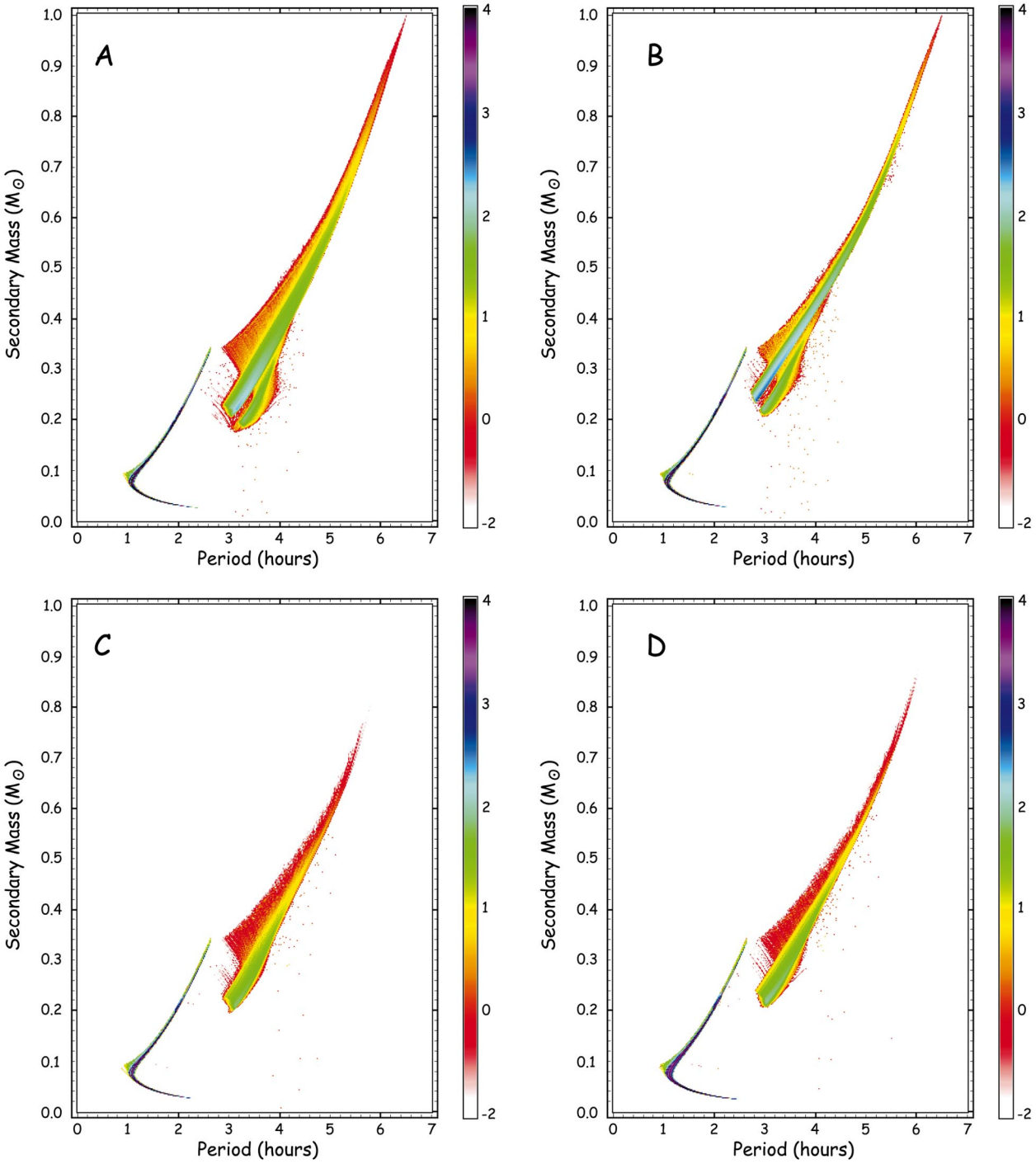

FIG. 12.—Same as Fig. 5, except that in addition to the standard model (*a*), the results for three other models are shown (see Tables 1 and 2): (*b*) reduced magnetic braking constant; (*c*) specific angular momentum lost with the ejected matter is twice that of the white dwarf; and (*d*) conservative mass transfer and retention by the white dwarf.

In Figure 13 we plot the polynomial fits that we made to the upper branches in the M_2-$P_{\rm orb}$ plane for the four different models. For comparison we show the M_2-$P_{\rm orb}$ relation that would be obtained if the donor star followed a main-sequence radius-mass relation (the one derived from our bipolytrope code). This set of curves shows quantitatively how mass determinations based solely on $P_{\rm orb}$ are affected by the thermal bloating effect. Note how the effect should go from a maximum at ~ 3 hr to quite small at $P_{\rm orb} \sim 5.5$ hr.

Finally, we point out that if, in fact, the period gap is in any way related to a relaxation from thermal bloating, then the inferred effect on mass determinations based on the orbital period must be approximately in the range of 25%–50%. To demonstrate this, we note that in the basic paradigm for producing the period gap, the system masses do not change from the upper boundary of the gap ($P_{\rm upper}$) to the lower boundary ($P_{\rm lower}$), while the radius shrinks from its bloated state, characterized by a bloating factor, f, to nearly its main-sequence radius at the lower edge of the gap.

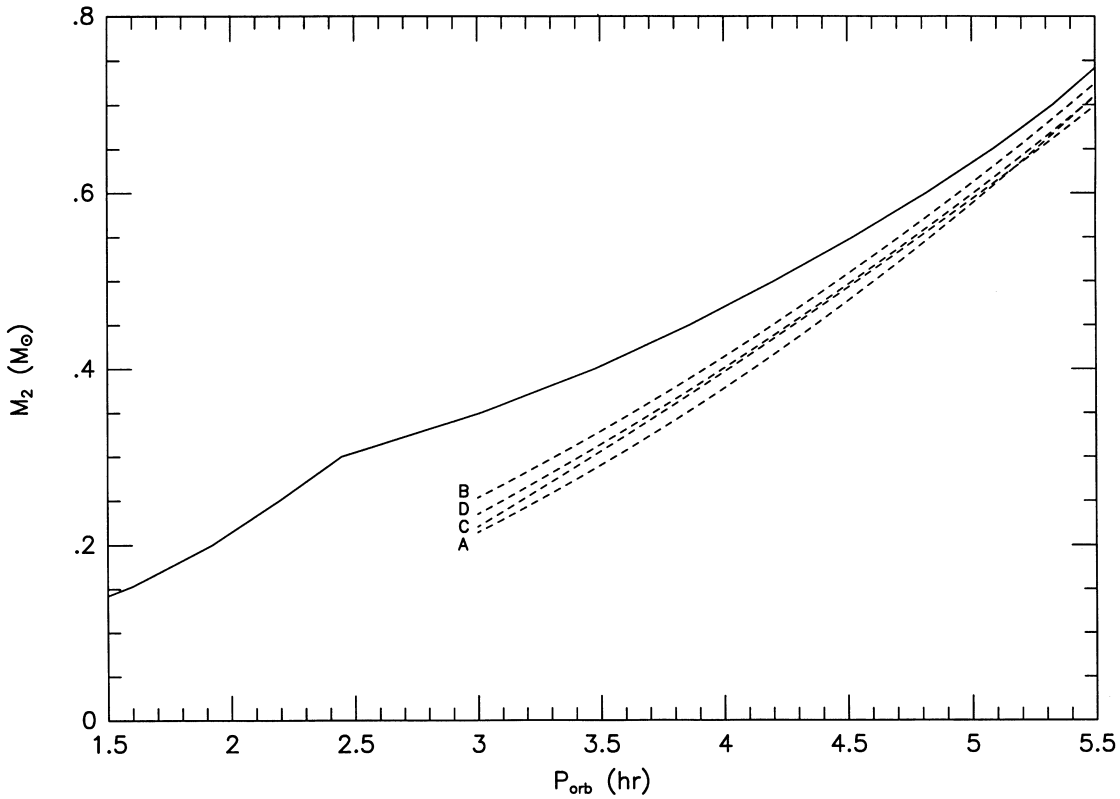

FIG. 13.— Secondary (donor) mass, M_2 as a function of orbital period. The solid curve is based on the assumption that the donor star fills its Roche lobe and has a radius-mass relation appropriate to stars on the main sequence (i.e., eq. [2]) The main-sequence models were generated with the same bipolytrope code that was used to carry out the binary stellar evolution calculations and are discussed in the text. The dashed curves are polynomial fits to the M_2-$P_{\rm orb}$ relations derived from the population synthesis study shown in Fig. 12. The labels (*a*)–(*d*) correspond to the four different panels in Fig. 12.

A simple application of Kepler's third law for the case of a Roche lobe filling star (which is true at both the upper and lower edges of the gap) shows that

$$f = \left(\frac{P_{\rm upper}}{P_{\rm lower}}\right)^{2/3}, \qquad (13)$$

where f must range from $\sim$1.2–1.3, depending on whether the period gap is taken to be $\frac{3}{4}$ hr or 1 hr in width, respectively (we have assumed that the gap is centered at 2.5 hr). From equation (6) we see that this value of f should reduce the inferred mass, at the top edge of the period gap, by amounts ranging from $\sim$30%–40%, in basic agreement with our more detailed population synthesis study. (For a related discussion see Beuermann et al. 1998.)

This type of discrepancy between the mass inferred for a secondary star, based on the CV orbital period and the assumption that its radius is that of a main-sequence star, has probably already led to a number of incorrect mass determinations reported in the literature, particularly for systems with $P_{\rm orb}$ between 3–5.5 hr. For example, at an orbital period of 3.2 hr, the mass assigned to a CV secondary would be 0.35 $M_\odot$, while our calculations show that it would actually be only 0.26 ± 0.02 $M_\odot$, although bloated in size. For a known or inferred mass ratio of, say, $q = 0.4$, we would then calculate a white dwarf mass of 0.89 $M_\odot$, when the true white dwarf mass is only 0.65 $M_\odot$. Thus, ignoring the bloating effect in the secondary stars in CVs with orbital periods of 3–5 hr can lead to a significant overestimation of both component masses.

It is interesting to note here that the secondary stars that are farthest from thermal equilibrium are those in systems with orbital periods just above the period gap (see Figs. 4, 5, and 13). Observationally, this orbital period region (3–4 hr) essentially contains only high mass transfer rate, nova-like (NL) types of CVs. The inferred high mass transfer rates for these systems would then be expected, on theoretical grounds, to lead to a large bloating of the secondary stars and, hence, to lower masses than might otherwise be anticipated. Precise observational determinations of the secondary star masses in NLs would allow a confirmation of this basic effect, which is, in fact, required if the period gap is to be explained by the interrupted magnetic braking scenario.

Figure 13 provides our theoretical predictions for the most likely mass of the secondary star at any given orbital period (see Table 2). Observational determinations accurate to a few percent would be needed in order to differentiate between the four models presented; but, accuracies of only $\sim$10% will allow a test of the bloating model in general and of the predicted deviation of the donor star from the main sequence. This is a challenging observational project, however, since the systems with orbital periods in the 3–5 hr range are ones in which the secondary star is rarely directly observed. IR spectral studies (e.g., Howell, et al. 2000; Mason, et al. 2000; Dhillon et al. 2000) have looked in detail for the secondary star in a number of CVs with only marginally successful results. In these CVs, spectral identification of absorption features due to the secondary star is difficult since the lines are rotationally broadened and filled in by radiation from the accretion disk. For the critical 3–5 hr period range, a signal-to-noise ratio of greater than 100 in the continuum will be needed to allow the atomic and molecular features of the secondary to be observed against the high background accretion-disk–dominated continuum.

We therefore advocate high signal-to-noise, orbital phase-resolved, near- and mid-IR spectroscopic observations with large ground-based telescopes (e.g., Gemini, Keck), and eventually with *SIRTF*, of sources such as the brightest NLs and other CVs, which have $P_{\rm orb} = 3$–5 hr.

7. SUMMARY AND CONCLUSIONS

In this paper we briefly reviewed our current understanding of the secular evolution of CVs through their mass transfer phase, including the currently accepted model for the 2–3 hr "period gap" in the orbital period distribution. The results of evolution calculations for a representative sample of individual systems are presented, as functions of both time and orbital period. A population synthesis code, which starts with some 3×10^6 primordial binaries, was then used to generate $\sim 2 \times 10^4$ systems that evolve successfully through the CV phase of mass transfer. This allows for a more complete exploration of parameter space. The results are displayed as probability densities in the $\dot{M}$-$P_{\rm orb}$, M_2-$P_{\rm orb}$, R_2-$P_{\rm orb}$, q-$P_{\rm orb}$, and $T_{\rm eff}/L_2$-$P_{\rm orb}$ planes for CVs at the current epoch. This method of displaying the results can lead to considerable insight into the relationships among the various system parameters. We find that for CVs with orbital periods above 5.5 hr and below the period gap (but above the period minimum) the secondary stars closely follow the main-sequence R-M relation (cf. Beuermann et al. 1998). However, for those with $P_{\rm orb}$ between 3–5.5 hr, the effect of bloating causes them to deviate substantially from this same relation.

Among our more interesting results, we have shown that the donor star masses in CVs with orbital periods just above the period gap should be as much as 30%–50% lower than would be inferred on the assumption that the donor stars obey a main-sequence radius-mass relation. This conclusion is only valid if the basic underlying cause of the period gap is thermal bloating of the donor star for systems above the period gap (see §§ 1–6). On the basis of our results, we have proposed a direct observational test of, in particular, the basic paradigm of the period gap and, more generally, our overall understanding of the evolution of CVs. This test involves the challenging, but realistic, task of making relatively accurate (e.g., 10%) determinations of the secondary masses in about a half-dozen CVs in the period range of 3–4 hr. If the masses are consistent with the assumption of a main-sequence radius-mass relation for the donor stars, then the currently accepted explanation of the period gap cannot be correct and the very existence of the gap would pose a major conundrum. If, on the other hand, the masses are mostly consistent with the lower values predicted in this work, then a substantial part of our basic understanding of the secular evolution of CVs will be validated.

Previously, much observational attention in CV studies has been focused on determinations of the white dwarf masses. While this is clearly of great interest, we hope with this work to stimulate more interest in the important issue of determining the secondary masses.

This research was supported in part by NASA under ATP grants GSFC-070 and NAG 5-8500 (to S. B. H.) and NAG 5-7479 and NAG 5-4057 (to S. A. R.). L. A. N. acknowledges the financial support of NSERC (Canada) and thanks CITA and the University of Toronto for a Reinhardt Fellowship and for their hospitality. We thank M. Politano for a number of useful discussions relating to this work. We are grateful to an anonymous referee who made numerous helpful and insightful comments that led to significant improvements in the paper. We also thank D. MacCannell and G. Esquerdo for their technical assistance.

REFERENCES

Abt, H. A., & Levy, S. G. 1978, ApJS, 36, 241
Alexander, D. R., Johnson, H. R., & Rypma, R. L. 1983, ApJ, 272, 773
Baraffe, I., Chabrier, G., Allard, F., & Hauschildt P. H. 1998, A&A, 337, 403
Beuermann, K., Baraffe, I., Kolb, U., & Weichhold, M. 1998, A&AS, 339, 518
Burrows, A., Hubbard, W. B., Saumon, D., & Lunine J. I. 1993, ApJ, 406, 158
Burrows, A., et al. 1997, ApJ, 491, 856
Clemens, J. C., Reid, I. N., Gizis, J. E., & O'Brien, M. S. 1998, ApJ, 496, 352
de Kool, M. 1992, A&A, 261, 188
Dhillon, V., Littlefair, S., Howell, S. B., Ciardi, D., Harrop-Allin, M. K., & Marsh, T. 2000, MNRAS, 314, 826
Di Stefano, R., & Rappaport, S. 1994, ApJ, 423, 274
Dorman, B., Nelson, L., & Chau, W. 1989, ApJ, 342, 1003 (DNC)
Duquennoy, A., & Mayor, M. 1991, A&A, 248, 485
Eggleton, P. 2001, in ASP Conf. Ser. 229, Evolution of Binary and Multiple Star Systems, ed. Ph. Podsialowski, S. Rappapart, A. King, F. D'Antona, & L. Burdieri (San Franciso: ASP)
Faulkner, J. 1971, ApJ, 170, L99
Halbwachs, J. L. 1987, A&A, 183, 234
Hameury, J. M., King, A. R., Lasota, J. P., & Ritter, H. 1988a, MNRAS, 231, 535
———. 1988b, ApJ, 327, 77
Howell, S. B., Ciardi, D., Dhillon, V., & Skidmore, W. 2000, ApJ, 530, 904
Howell, S. B., Rappaport, S., & Politano, M. 1997, MNRAS, 287, 929 (HRP)
Howell, S. B., Szkody, P., & Cannizzo, J. 1995, ApJ, 439, 337
Joss, P. C., Rappaport, S., & Lewis, W. 1987, ApJ, 319, 180
Kippenhahn, R., Kohl, K., & Weigert, A. 1967, Z. Astrophys., 66, 58
Kolb, U. 1993, A&AS, 271, 149
Kolb, U., King, A., & Ritter, H. 1998, MNRAS, 298, L29
Kopal, Z. 1959, Close Binary Systems (London: Chapman & Hall)
Krishna-Swamy, K. S. 1972, PASP, 84, 64
Landau, L.D., & Lifshitz, E.M. 1962, The Classical Theory of Fields (2d ed.; Oxford: Pergamon)
Livio, M., & Soker, N. 1988, ApJ, 329, 764
Lynden-Bell, D., & Pringle, J. E. 1974, MNRAS, 168, 603
Mason, E., Skidmore, W., Howell, S. B., Ciardi, D., Littlefair, S., & Dhillon, V. 2000, MNRAS, 318, 429
Mennickent, R. Matsumoto, K., & Arenas, J. 1999, A&A, 348, 466
Meyer, F., & Meyer-Hofmeister, E. 1979, A&A, 78, 167
Miller, G. E., & Scalo, J. M. 1979, ApJS, 41, 513
Nelson, L. A., Rappaport, S. A., & Joss, P. C. 1986a, ApJ, 304, 231
———. 1986b, ApJ, 311, 226
———. 1993, ApJ, 404, 723
Paczyński, B. 1965, Acta Astron., 15, 89
———. 1967, Acta Astron., 17, 193
———. 1976, in IAU Symp. 73, Structure and Evolution of Close Binary Systems, ed. P. Eggleton, S. Mitton, & J. Whelan (Dordrecht: Reidel), 75
Paczyński, B., & Sienkiewicz, R. 1981, ApJ, 248, 27
Patterson, J. 1984, ApJS, 54, 443
Politano, M. 1988, Ph.D. thesis, Univ. Illinois
———. 1996, ApJ, 465, 338
Prialnik, D., & Kovetz, A. 1995, ApJ, 445, 789
Rappaport, S., Di Stefano, R., & Smith, J. D. 1994, ApJ, 426, 692 (RDS)
Rappaport, S., Joss, P. C., & Webbink, R. F. 1982, ApJ, 254, 616 (RJW)
Rappaport, S., Verbunt, F., & Joss, P. C. 1983, ApJ, 275, 713 (RVJ)
Salpeter, E. 1955, ApJ, 121, 161
Schenker, K., Kolb, U., & Ritter, H. 1998, MNRAS, 297, 633
Shara, M., Livio, M., Moffat, A., & Orio, M. 1986, ApJ, 311, 163
Smith, D. A., & Dhillon, V. S. 1998, MNRAS, 301, 767
Spruit, H. C., & Ritter, H. 1983, A&A, 124, 267
Starrfield, S. 1998, in ASP Conf. Ser. 137, Wild Stars in the Old West, ed. S. Howell, E. Kuulkers, & C. Woodward (San Francsico: ASP), 352
Taam, R. E., Bodenheimer, P., & Ostriker, J. P. 1978, ApJ, 222, 269
Taam, R. E., & Sandquist, E. 1998, in ASP Conf. Ser. 138, Pacific Rim Conference on Stellar Astrophysics, ed. K. L. Chan, K. S. Cheng, & H. P. Singh (San Francisco: ASP), 349
Verbunt, F. 1997, MNRAS, 290, L55
Verbunt, F., & Zwaan, C. 1981, A&A, 100, L7

Warner, B. 1976, in IAU Symp. 73, Seventh International Colloquium on UV and X-Ray Spectroscopy of Astrophysical and Laboratory Plasmas, ed P. K. Carroll (Dublin: Univ. Dublin, Physics Dept.), 85
———. 1995, Cataclysmic Variable Stars (New York: Cambridge Univ. Press), chap. 2
Webbink, R. F. 1979, in IAU Colloq. 53, White Dwarfs and Variable Degenerate Stars, ed. H. van Horn & V. Weidemann (Rochester: Univ. Rochester Press), 426
Webbink, R. F. 1985, in Interacting Binary Stars, ed. J. E. Pringle & R. A. Wade (Cambridge: Cambridge Univ. Press), 39
———. 1992, in X-Ray Binaries and Recycled Pulsars, ed. E. P. J. van den Heuvel & S. Rappaport (Dordrecht: Kluwer), 269
Webbink, R. F., Livio, M., Truran, J. W., & Orio, M. 1987, ApJ, 314, 653
Wheatley, P. J. 1995, MNRAS, 274, L51
Wickramasinghe, D. T., & Wu, K. 1994, ApJS, 211, 61